ISSN 2354-9114 (online), ISSN 0024-9521 (print)
Indonesian Journal of Geography Vol 55, No 1 (2023): 10-29
DOI: 10.22146/ijg.76433 website: https://jurnal.ugm.ac.id/ijg
©2023 Faculty of Geography UGM and The Indonesian Geographers Associaton

INDONESIAN JOURNAL OF GEOGRAPHY

RESEARCH ARTICLE

Groundwater Chemistry Characterization in The South and Southeast Merapi Volcano, Indonesia

Heru Hendrayana[1*], Agung Harijoko[1], Indra Agus Riyanto[2], Azmin Nuha[3], Ruslisan[4]
[1]Geological Engineering Department, Faculty of Engineering, Universitas Gadjah Mada, Indonesia.
[2]Environmental Geography, Faculty of Geography, Universitas Gadjah Mada, Indonesia.
[3]Groundwater Working Group (GWWG), Faculty of Engineering, Universitas Gadjah Mada, Indonesia.
[4]GIS Department Wilmar Nabati, Indonesia.

Received : 2022-07-20
Revised: 2022-09-11
Accepted: 2023-01-23

Keywords: Aquifer system, Merapi Volcano, Groundwater Chemistry, Landuse Change, Water Table Decline

Correspondent email: heruhendrayana20@gmail.com

Abstract. Merapi Volcano, which differs from volcanoes in other climates due to its location on the Indonesian Maritime Continent influenced by ENSO, ICTZ, and Moonsons, plays an essential role as a source of groundwater for the surrounding population. Some problems associated with groundwater in Mount Merapi are high utilization compared to other volcanoes worldwide, changes in land use, pollution, and its lowering table. Therefore, this study aims to compare the hydrogeological characteristics and aquifer systems of the southern and southeastern parts of Merapi Volcano. The hydrogeological characteristics were obtained from geological mapping, surface and subsurface, as well as rock XRF tests. Meanwhile, the hydrogeochemical characterization was determined through chemical data using the Trilinear Piper, Kurlov, Fingerprint, Composition, and Harker Diagram methods. The results of the Trilinear Piper, Kurlov, Fingerprint, and Composition Diagram methods show that Mount Merapi has 3, 7, 4, and 2 types of patterns different from other volcanoes in the world. On the other hand, the Harker diagram has the same pattern of Mg-Ca and Mg-Na as several other volcanoes. In conclusion, the hydrostratigraphy in the southern part of the volcano, consists of aquifuge, aquiclude, and aquifer, while in the southeast, there are aquitards of volcanic sandstone and tuff.

©2023 by the authors. Licensee Indonesian Journal of Geography, Indonesia.
This article is an open access article distributed under the terms and conditions of the Creative Commons Attribution(CC BY NC) licensehttps://creativecommons.org/licenses/by-nc/4.0/.

1. Introduction

Volcanoes offer several benefits to the surrounding community in terms of fertile soil and abundant water sources. Innumerable preliminary studies reported that groundwater resources are found in volcanic aquifer layers (Revil et al., 2004; Join et al., 2005; Delcamp et al., 2016; Fenta et al., 2020). Fortunately, these are characterized by porous medium and high productivity (Fetter, 2000; Todd & Mays, 2005). As a result, people worldwide tend to use groundwater in the vicinity of a volcanic eruption as the primary water source (UNESCO, 2004; Siebert et al., 2010; Margat & Gun, 2013). According to Demlie et al. (2007), Herrera and Custodio (2008), Mulligan et al. (2011), and Ureta et al. (2020), groundwater around volcanoes is widely used because of its good quality and accessibility.

Zaenudin (2010) stated that Indonesia is one of the countries with the highest number of volcanoes, approximately 129. This country usually experiences high rainfall in the tropics. Therefore, it has abundant groundwater potential. According to Hendrayana et al. (2020, 2021), the groundwater resources in Merapi Volcano are widely used to meet the people's water needs, especially those from Sleman, and Bantul Regencies and Yogyakarta Cities in Yogyakarta Province as well as Magelang, Boyolali, and Klaten Regencies in Central Java. This plays a vital role, and sustainable management is necessary. It requires aquifer configuration, hydrogeochemical and hydro-isotope data, groundwater fluctuations, usage, and quality (Hadian et al., 2016; Toulier et al., 2019; Baud et al., 2021).

The volcanoes in Indonesia are unique compared to those found in other parts of the world. Cahyadi et al. (2021) stated that these are usually located on the Indonesian Maritime Continent, and it affects the high rainfall triggered by Monsoons, El Niño Southern Oscillation (ENSO), and Inter Tropical Convergence Zone (ITCZ) (Aldrian & Susanto, 2003). Döll and Fiedler (2008) reported that the high tropical rainfall impacts the potential for groundwater recharge, especially in volcanoes. On the southern slope, those in the central zone of Java experience extremely high rainfall compared to the northern part (Qian et al., 2010). This has certain implications compared to the amount of recharge on the southern slope. Merapi Volcano has similar characteristics. The southern part has high rainfall, while the northern slope has low rainfall because it is located in the rain shadow zone. Interestingly, this area experiences an annual average rainfall of > 3,000 mm/year (Wredaningrum & Sudibyakto, 2014), which is higher than those in other climatic regions. For example, Mt Vulture Italy, 850 mm/year (Parisi et al., 2011), Mt Cimino Italy, 1084 mm/year (Piscopo et al., 2018), Mt Wonchi Ethiopia 1,400 mm/year (Kebede et al., 2008), Yellowstone Volcano USA 450 mm/year (Gray et al., 2007), and Fuji Volcano Japan 1,500 mm/year (Sugiyama et al., 2016).

Additionally, groundwater utilization in the southern part of Mount Merapi is quite high, relatively 100 x 106 m3/year (Hendrayana, 1993; Hendrayana & Vicente, 2013). This is higher than other volcanoes in the world, such as Mt Epomeo Italy, 18 x 106 m^3/year (Piscopo et al., 2020), Mt Real de Telde 24 x 106 m^3/years (Cabrera & Custodio, 2004), Mt Halla Jeju Island South Korea 240 x 106 m^3/years (El-Kadi et al., 2014) and Mt Sierra De Guanajuato Mexico 700 x 106 m^3/year (Mahlknecht et al., 2004). Several problems are associated with lowering the groundwater table (Hendrayanan et al., 2021; Wilopo et al., 2021) and pollution on the southern and southeastern slopes (Putra, 2015; Fathmawati et al., 2017). Additionally, the pattern of land use change at Mount Merapi is relatively dynamic (Rahardian & Buchori, 2016; Sarminingsih et al., 2018) compared to other volcanoes in the world.

The present study aims to compare the characteristics of groundwater chemistry in the southern and southeastern sections of Merapi Volcano based on the condition of its aquifer system. In the southern section, there have been massive changes in land use for residential areas. The quantity of extracted groundwater from relatively 849 drilled wells is used to meet the water needs of hotels, offices, and industries, and it is pumped at approximately 340,000 m^3/day. Interestingly, the southeastern area is featured by the transition (meeting point) of Young Deposits of Merapi Volcanic (Quarternary) and the Kebobutak Formation (Tertiary) materials – sandstone, claystone, and tuff (Rahardjo, 1995), thereby allowing the mixing process of groundwater to occur. According to Djaeni (1982), the transition area contains regions with unexploitable groundwater, even within extensive and productive aquifers.

The southeastern section is covered by 24% forest, with a massively undeveloped residential area. It also has few industries; therefore, groundwater extraction from drilled wells is relatively small. The population is quite dense, with a total of 1,200,000 residents compared to that of the southern section of only 550,000 people (BPS, 2021). Groundwater is the primary source of clean water in the southern and southeastern areas. Related studies comparing several sections of volcanic slopes are rarely carried out because these are generally located within the same geological formation (Santosa & Sutikno, 2006; Selles, 2014; Poetra et al., 2020).

Hydrogeological and hydrogeochemical studies characterize groundwater chemistry and conceptual design models of aquifer systems. The results are needed to determine the activities required for the sustainable management of groundwater, which is essential (Kulkarni et al., 2004; Sophocleous, 2010; Riyanto et al., 2020). Several standard measures in management programs limit land-use changes, prevent groundwater table decline, and limit usage (Sophocleous, 2005; Fackrell et al., 2020; Bremer et al., 2021). Irrespective of the fact that both are within the same section of Merapi Volcano, the two studies possess different environmental characteristics, thereby making it necessary to have various groundwater management programs for each site.

The study area is divided into the southern and southeastern sections. Figure 1 shows that the southern and southeastern sections are located in the Special Region of Yogyakarta, and Central Java Provinces, respectively. Exhaustively, the southern and southeastern areas are situated within the Gajahwong, and Dengkeng Watersheds, respectively. All study sections have Oldeman climate classification type B2 (moderate tropical rain forest) and C2 (moderate annual plantations) (Wredaningrum & Sudibyakto, 2014). The two regions have a slope grade within the range of five to 45% (Santosa & Sutikno, 2006), with predominant land uses for residential areas, rice, and dry fields (Herdiansyah et al., 2020),

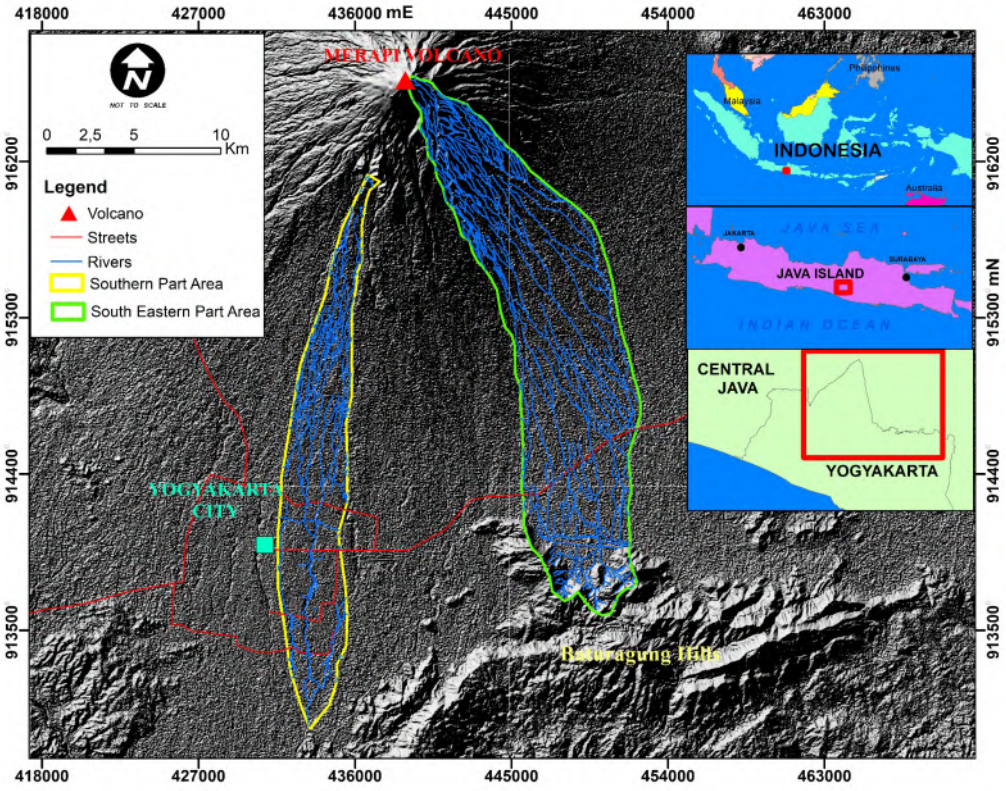

Figure 1. Study Area
(Basemap Sources: Indonesian Geospatial Agency-BIG, 2004)

including soil types of Hapludalfs Hapluderts, Udivitrands Udorthents, Ustipsamments Haplustands, Haplustepts Ustipsamments (Ministry of Agriculture, 2000). The southern and southeastern sections are located within the Yogyakarta-Sleman and Karanganyar-Boyolali Groundwater Basins. The study area is located in the aquifer's highly productive classes (Hendrayana et al. 2020, 2021).

Van Bemmelen (1949) stated that the study area is generally located within an active volcanic zone. A part of the Quaternary volcanic zone in the central part of Java Island (Pannekoek, 1949). Geomorphologically, the study area includes the following zones volcanic cone, slope, foot plain, and plain (Verstappen, 2000). Geologically, it consists of three formations, namely Lava Dome and Flows (d), Old Volcanic Deposits of Merapi Volcano (Qmo), and Young Deposits of Merapi Volcano (Qmi) (Rahardjo, 1995). The study area was affected by the eruption of the Merapi volcano from 1920 to 2010 (De Bélizal et al., 2013). The Qmo Formation comprises of breccia, agglomerate, and lava flows, as well as andesite and basalt-olivine. The Qmi Formation consists of undifferentiated tuff, ash, breccia, agglomerate, and lava flows. The southeastern section consists of pyroclastic deposits, such as block and ash flow deposits, andesitic lava, tephra, tuff, debris avalanche, detrital, and alluvial fans (Selles et al., 2015). The study area is located in the volcanic facies' central, proximal, medial, and distal zones (Marfai et al., 2012).

2. Methods

The physical properties of groundwater include temperature, electric conductivity (EC), total dissolved solids (TDS), and pH, which were directly measured on the field using a portable water checker (HI9813-6, Hanna, USA). These features were measured from 21 springs, 113 dug, and 16 deep wells. Groundwater table measurement was carried out simultaneously to measure its physical properties. The table elevation procedure was obtained by subtracting the topographic elevation from the depth of the groundwater table. The depth measurement was carried out using an automatic groundwater table sounding. Topographic data were obtained from the Shuttle Radar Topography Mission (SRTM) image. Visualization of the groundwater's physical properties was processed using the interpolation method in ArcGIS 10.8 Software. The Root Mean Squared Error (RMSE) of this procedure showed a small value (Ohmer et al., 2017). The groundwater table elevations from the measurement points were further processed using the interpolation method to generate the flow pattern map. The next step was to determine the samples for the groundwater chemistry test based on temperature, EC, TDS, pH, and groundwater flow direction distribution. Fortunately, 27 samples were realized from dug wells, 10 representatives from springs, and 11 from deep wells to be tested in the laboratory. The collected samples were tested using Na^+, Ca^{2+}, Mg^{2+}, Cl^-, CO_3^-, HCO_3^-, and SO_4^{2-} ion parameters. A groundwater chemistry characterization study is essential to discern or distinguish its features (Appelo & Postma, 2005).

The laboratory test results were then re-tested using Charge Balance Error (CBE) analysis, which showed that its maximum value was < 10% (Hiscock & Bense, 2014). The results were further processed using Rockworks 14 software, Trilinear Piper, Fingerprint Diagrams, and Kurlov Classification tools. The Trilinear Piper and Fingerprint Diagrams, as well as the Kurlov Classification, provided an overview of the groundwater type and its characteristics by analyzing its anion and cation concentrations. It was realized with the Composition Diagram tool using the Rockworks 14 Software. This analysis was intended to compare the concentration of each ion that constitutes the groundwater to the Total Dissolved Ion (TDI) to determine groundwater mixing. The subsequent step entails comparing the cations with rock X-Ray Fluorescence (XRF) results. The analysis results in the laboratory were converted into meq/litre units. The evaluation of the origin of groundwater needs to be supported by XRF data – to examine rock mineral elements and hydrogeochemical information (Oyedotun et al., 2018). The Harker Diagram was then generated using Microsoft Excel to identify the relationship between rock minerals and groundwater chemistry. The number of XRF rock samples analyzed in the laboratory was 10. These were selected based on a geological survey by observing outcrops in the field at 38 points. XRF rock samples were collected from the area using a geological hammer. Geological mapping was needed to detail the existing 1:100,000 scaled map (Rahardjo et al., 1995).

The next step was to complete the data needed to design a conceptual geological model based on the information on the recharge area resulting from the isotope analysis conducted by Wijatna et al. (2008), using a drill and geophysical information realized from Hendrayana (1993), Hendrayana and Vicente (2013), and Selles (2014). Fortunately, the conceptual model was built on hydro-stratigraphic units, aquifer type, and groundwater chemistry data. A study of temporal land-use changes, water license, groundwater usage, and table changes complemented the resulting model. Land-use change analysis was carried out based on images from Landsat five (1996), Landsat seven (2001, 2006, 2011), and Landsat eight (2006, 2021). The Landsat image was radiometrically and geometrically corrected using ENVI 5.3. The land-use identification was processed using ArcGIS 10.8 with the maximum likelihood algorithm. Land-use change analysis was carried out by comparing its annual dissimilarities. The data on licenses for deep groundwater extraction in 2019, 2020, and 2021 were obtained from the Yogyakarta and Central Java Province Tax Offices. Analysis of groundwater licensed extraction was conducted by comparing its uses under the same classification with that from a different year. Groundwater employed raw data in 2011, 2016, and 2021 from the Central Bureau of Statistics for the Special Region of Yogyakarta and Central Java Province. These were further analyzed using the formula standardized by the Indonesian National Standard (BSN, 2015), as shown in **Table 1**. During the final analysis, the changes in the groundwater table were carried out by comparing the results of the measured depth or elevation in 2021 and information from previous research.

3. Results and Discussion

The EC values within the range of 250 to 300 µS/cm were distributed following the same pattern in the southern and southeastern sections from the upper to the middle slope of Merapi Volcano. A similar distributive pattern within the range of 250 to 600 µS/cm was also detected at the lower slope or foot of the volcano, as shown in Figure 2. EC results with the same range of values 147 to 834 µS/cm were found in the De Fugo Guatemala Volcano (Mulligan et al., 2011). On the contrary, different results were found in Madeira Volcanic Island Portugal (Prada et al., 2005), Mount Vulture Italy (Parisi et al., 2011), Amiata Volcano Italy (Minnisale et al., 1997), Mt

Table 1. Groundwater Usage Calculation Formula

	Sectors	Equations	Remarks
1	Domestic	**365 days x {(qu/1000 x Pu) + (QR/1000 x Pr)}**	qu : water consumption in rural areas (60 litres/person/day). Pr: village/ rural population qr : water consumption in urban areas (120 litres/person/day). Pu : city population
2	Agricultures	**L x It x a**	L: area of irrigation It: crop intensity in per cent (%) season/year (120 days) A: water use standard (1 litre/sec/ha)
3	Livestock	**365 days x {q(c/b) x P(c/b) + q(pi) x P(pi) + q(PO) x P(PO)}**	q (c/b): water for cows/buffalo (40 litres/head/day) q (s/g): water use for sheep/goats (5 litres/head/day) q (pi) : water use for pigs (6 litres/head/day) q (PO) : water use for poultry (0.6 litre/head/day) P (c/b): number of cows/buffalo (head) P (s/g): number of sheep/goats (head) P (pi): number of pigs (head) P (PO) : number of birds (head)
4	Education	**365/1000 x m x Ss**	m : number of students Ss: standard of water consumption for schools (10 litres/student/day)
5	Hospital	**365/1000 x k x Sr**	k: number of rooms Sr: hospital water consumption standard (300 litres/room/day
6	Worship Facility	**365/1000 x ti x Si**	ti: number of places of worship Si: standard of water consumption for places of worship (3000 litres/ unit/day)
7	Restaurant	**365/1000 x r x Sr**	r: number of restaurants Sr: standard of water consumption for restaurants (100 litres/seat/day)
8	Hotel	**365/1000 x k x Sh**	k: number of rooms (10 rooms) Sh: standard water consumption for hotels (150 litres/room/day)
9	Fishery	**365/1000 x q(f) x A (FP) x 1000**	q(f): flashy water use (7 mm/ha/day) A (FP): pond area (ha)
10	Industry	**365/1000 x p x Si**	Q: number of employees Si: standard of water consumption for industry (10 litres/person/day)

Source : (BSN, 2015 with modification)

Etna Italy (Bellia et al., 2015), and Fantale Volcano in Ethiopia (Furi et al., 2012) with values of 109 to 3,300 µS/cm, 190 to 1,330 µS/cm, 141 to 1,149 µS/cm, 219 to 2,300 µS/cm, and 109 to 2,060 µS/cm.

The difference in EC distribution was discovered in the southern section with values of 600 to 750 µS/cm. This was caused by an increase in groundwater pollution in Yogyakarta City. Incidentally, this phenomenon follows the findings of Fathmawati et al. (2018) in densely populated areas in Yogyakarta City, where septic tank leakages and domestic sewage caused an increase in groundwater pollution, thereby raising the nitrate value by 50 to 100 mg/litre. There is a correlation between nitrate pollution and EC value in Yogyakarta City. According to Kämpfner et al. (2021), the higher the nitrate value, the greater the EC. In the southeastern section, a high EC value within the range of 900 to 1,200 µS/cm was found in the foot plains, which was caused by connate water traps. The result is in line with Lisan and Adji (2017) research, that high EC and low resistivity values of 1,200 to 2,500 µS/cm and 0 to 1 Ω m were found in the southern section. The presence of connate water traps was caused by the lifting process of the southern mountains that formed the Gantiwarno Swamp and trapped seawater during the Pliocene period (Rahardjo 2000).

Different pH values are distributed in the southern and southeastern sections. In the southern section, values within the range of 6.5 to 7 are found on the upper slope of the foot of Merapi Volcano. In the southeastern section, pH values of 6.5 to 7 are detected in the upper and middle slopes. However, pH results with the same range of values 6.1 to 7 (Mulligan et al.2, 2011), and 6.13 to 7.55 (Minnisale et al., 1997), were found in De Fugo and Amiata Volcanoes in Guatemala, and Italy, respectively. Lower pH values of 5.9 to 6.3 (Parisi et al., 2011), and 6.08 to 6.82 (Afsin et al., 2014), were found at Mount Vulture and Hasandagi Volcano and Turkey, respectively. Higher pH values of 6.2 to 8.4 (Prada et al., 2005), 6.4 to 8.44 (Bellia et al., 2015), and 7.3 to 8.2 (Furi et al., 2012), were found in Madeira Volcanic Island, Portugal, Mt Etna, Italy, and Fantale Volcano, Ethiopia, respectively.

In the southern section, especially on the plain of Merapi Volcano, the pH of 6.20 to 6.5 is due to pollution in Yogyakarta City. These results align with the findings of Kämpfner et al. (2021) that groundwater pollution in Yogyakarta City reduces the pH value. A different pattern was discovered in the southeastern section, where connate water traps caused high pH values of 7 to 7.6. These results are in line with the findings of Nasr and Zahran (2014) that there is a relationship between pH and TDS. Furthermore, the TDS values in the southeastern section are high, > 600 ppm, but low in terms of classifying groundwater as brackish (McNeely et al., 1979). Therefore, the high TDS values cause a rise in the high pH detected in the southeastern section.

The TDS in the southern section is <125 ppm from the upper to the middle slope of Merapi Volcano. Meanwhile, from the lower slope to the plain, the TDS values range from 126 to 250 ppm. There is an interesting pattern in the southern section, which has high TDS values of 251 to 375 in Yogyakarta City due to groundwater pollution. In this area, the TDS values < 150 ppm are found in the upper slopes of the foot of Merapi Volcano. On its plain, its value is within the range of 151 to 300 ppm. A unique pattern of high-value TDS was found in the southeastern section ranging from 301 to 450 ppm and 450 to 600 ppm, influenced by connate water traps. TDS results with similar values of 9.4 to 796 ppm as the study location were found in the Mexican volcanoclastic aquifer (Hernández-Pérez et al., 2022). Different TDS values with a larger range of 302 to 1,583 ppm (Morales-Casique, 2012), 149 to 1,693 ppm (Bellia et al., 2015), 287 to 1,814 ppm (Furi et al., 2012), 546 to 2,412 ppm (Parisi et al., 2011), 166 to 4,723 ppm (Afsin et al., 2014), and 118 to 5,342 ppm (Minnisale et al., 1997), are found in Popocatépetl volcano, Mexico, Mt Etna Italy, Fantale Volcano, Ethiopia, Mt Vulture, Italy, Hasandagi Volcano, Turkey, and Amiata Volcano, Italy respectively.

The south and southeast sections exhibit similar temperature distribution patterns of 24 to 26 °C, 26 to 28 °C, and 28 to 30 °C in the upstream, middle and downstream. Temperature values within the same range as the study location were found in De Fugo Volcano, Guatemala, 20.9 to 25.3°C (Mulligan et al., 2011) and Hasandagi Volcano, Turkey, 20.5 to 29°C (Afsin et al., 2014). There are much higher temperature values at Fantale Volcano in Ethiopia of 27 to 39°C (Furi et al., 2012). In addition, there are lower temperatures compared to the Mount Vulture study site in Italy, 15.1 to 19.8°C (Parisi et al., 2011), Amiata Volcano in Italy, ranging from 8 to 23°C (Minnisale et al., 1997), Madeira Volcanic Island Portugal 10.1 to 28 °C (Prada et al., 2005), and MT Etna Italy 9 to 29°C (Bellia et al., 2015).

Hydrogeochemical Analysis Using The Trilinear Piper Diagram

The Trilinear Piper Diagram shows that the southern part has three groundwater types, namely calcium magnesium bicarbonate, alkali bicarbonate, and alkali chloride, as illustrated in Figure 3. The calcium magnesium bicarbonate type is present in 20 samples, as shown in Table 2, and characterized by Ca^{2+} + Mg^{2+} ions > Na^{+} + K^{+} and HCO_3^{-} > Cl^{-}+SO_4^{2-}. The alkali bicarbonate type is found in two samples

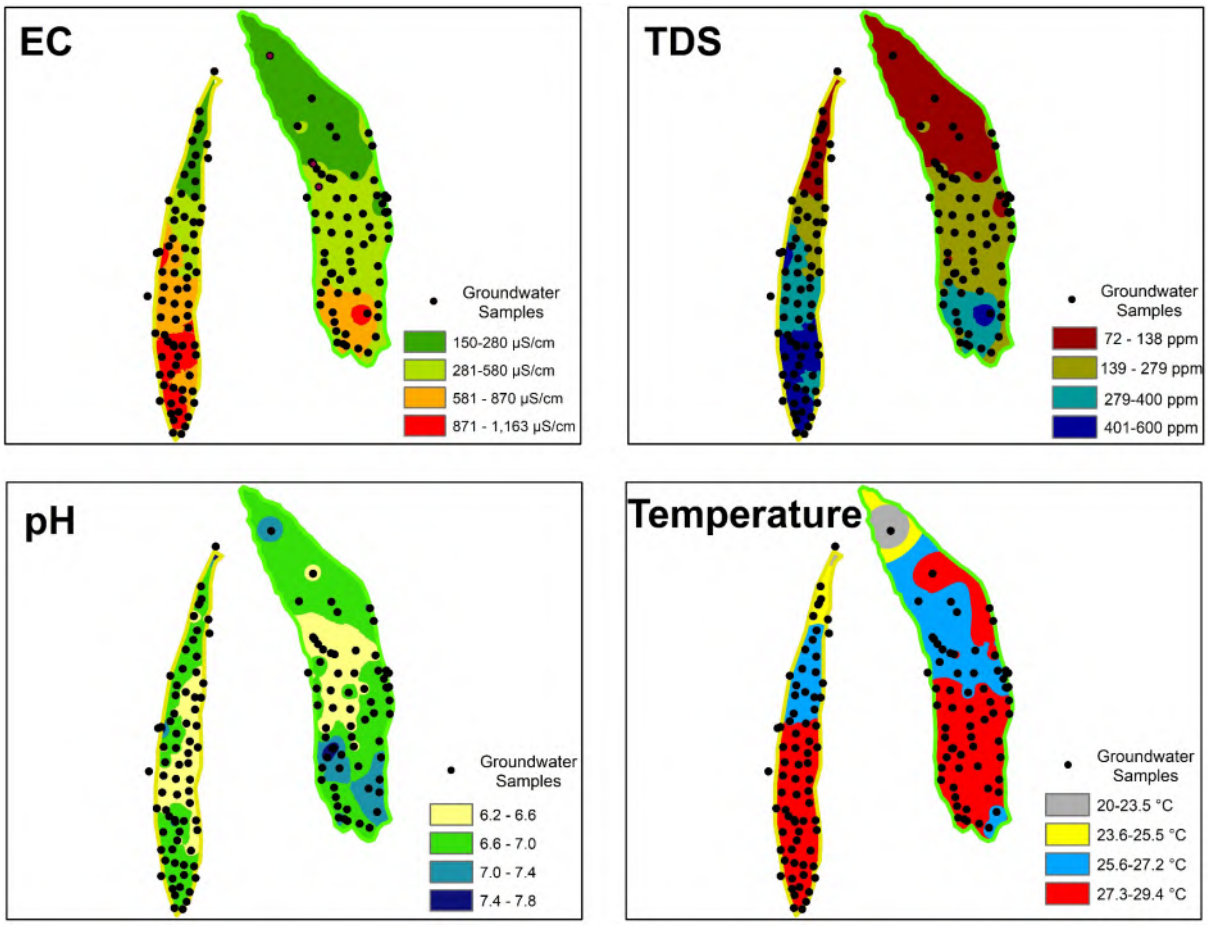

Figure 2. Map of Distribution of EC, TDS, pH, and temperature
(Basemap Sources: Indonesian Geospatial Agency-BIG, 2004)

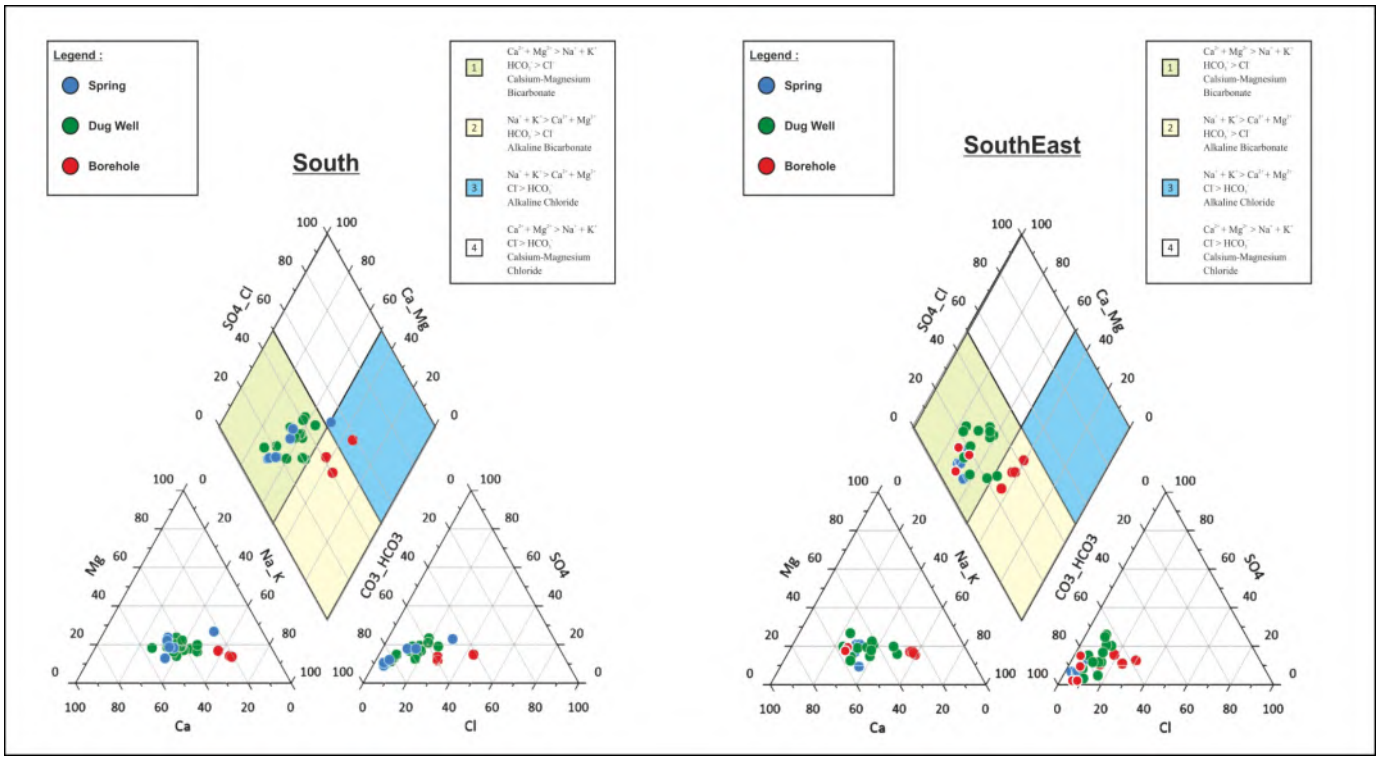

Figure 3. The Results of Trilinear Piper Diagram

(BH1-S and BH2-S) and has similar characteristics with ions $Na^+ + K^+ > Ca^{2+} + Mg^{2+}$ and $HCO_3^- > Cl^- + SO_4^{2-}$. The alkali chloride type is found in two samples (S 3-S and BH3-S) with the characteristics of $Na^+ + K^+ > Ca^{2+} + Mg^{2+}$ and $Cl^- + SO_4^{2-} > HCO_3^-$. The southeast and southern sections have the same groundwater types, namely calcium magnesium and alkaline bicarbonates comprising nine and five samples. Nevertheless, the southeastern section does not have an alkali chloride type (Table 3). The alkali bicarbonate type in the southeastern section is found in DW 5-SE, BH 10-SE, BH 11-SE, BH 12-SE, and BH 13-SE samples (Figure 4A).

The calcium magnesium bicarbonate type indicates that the groundwater originates from volcanic facies with high calcium and magnesium ions. The main minerals contained in volcanic rocks found in lava breccias and pyroclastic outcrops are plagioclase and pyroxene. When the carbonate ions are higher than the chloride, it indicates that the water emerges from shallow groundwater. The alkaline bicarbonate type depicts that the aquifer comprises loose andesite material containing high sodium and potassium ions. However, assuming the concentration of carbonate ions is higher than that of chloride, it simply depicts the water that emerges from shallow groundwater. The alkaline chloride type has the chemical properties of water derived from loose andesite fragments with high sodium and potassium ions. Supposing the concentration of chloride ions is higher than that of the carbonate, it simply implies that the water emerges from deep groundwater. Similar patterns of the Trilinear Piper Diagram in Indonesia were also found in Mount Ciremai (Irawan et al., 2009), Bromo-Tengger (Toulier et al., 2019), Mount Agung and Batur (Purnomo & Pichler, 2015), and Salak (Hadian et al., 2016). The same patterns of the Trilinear Piper Diagram outside Indonesia were also found in Mt Fuji, Japan (Ono et al., 2019), Mt Vulture, Italy (Parisi et al., 2011), Volcanic Island, Portugal (Prada et al., 2005), Yellowstone Plateau Vulcanic, USA (Hurwitz et al., 2007), and Mt De Fuego Guatemala (Mulligan et al., 2011). The results of all groundwater geochemical analyses in predominantly volcanic areas are categorized under the calcium-magnesium bicarbonate type.

Hydrogeochemical Facies Analysis using the Kurlov Classification

The Kurlov analysis of the southern section classifies groundwater into seven classes, namely calcium alkali bicarbonate (Ca^{2+}- Na^++K^+- HCO_3^-) – 14 samples, calcium alkali bicarbonate nitrate (Ca^{2+}- Na^++K^+- HCO_3^-- NO_3^-) – two pieces, alkali calcium bicarbonate nitrate (Na^++K^+- Ca^{2+}- HCO_3^-- NO_3^-) – one sample, alkali calcium bicarbonate (Na^++K^+- Ca^{2+} - HCO_3^-) – three pieces, alkali magnesium bicarbonate chloride (Na^++K^+ -Mg^{2+}- HCO_3^-) – one sample, alkali calcium bicarbonate chloride (Na^++K^+- Ca^{2+}- NO_3^--Cl^-) – one piece, alkali bicarbonate chloride (Na^++K^+- $HCO_3^-$$Cl^-$) – one sample, and alkali chloride bicarbonate (Na^++K^+- Cl^- - HCO_3^-) – one piece. Flow path 1 from the upper to the middle slope of Merapi Volcano is categorized in the calcium alkali bicarbonate (Ca^{2+}- Na^++K^+- HCO_3^-) class (Figure 4B). Flow path 2 on the lower slope changes its composition to calcium alkali bicarbonate nitrate. Flow path 3 in the transition region of the foot of the volcano changes to the alkali magnesium bicarbonate chloride. Flow path 4 at the foot of the volcano changes to the alkali calcium bicarbonate class. Flow path 5 at the end of the volcanic foot transition changes to the alkali calcium bicarbonate nitrate. Flow path 6 on the volcanic plain changes the groundwater type to alkaline chloride bicarbonate, alkaline bicarbonate chloride, and alkaline calcium bicarbonate chloride.

Table 2. Characteristics of Cations and Anions in The Southern Section of Merapi Volcano

Samples	Ion Concentration (meq/l)								Cation	Anion	TDI	CBE (%)
	K^+	Na^+	Mg^{2+}	Ca^{2+}	SO_4^{2-}	NO_3^-	Cl^-	HCO_3^-				
DW4-S	0.74	1.53	0.92	1.95	0.69	1.46	0.92	2.00	5.14	5.07	10.21	0.71
DW5-S	0.40	1.17	0.64	1.55	0.50	0.61	0.49	1.80	3.75	3.41	7.16	4.82
DW8-S	0.43	1.12	0.75	1.63	0.54	0.92	0.46	1.80	3.93	3.73	7.66	2.69
DW9-S	0.39	0.99	0.69	1.62	0.56	0.96	0.45	1.40	3.69	3.37	7.07	4.53
DW15-S	0.23	0.64	0.61	1.84	0.27	0.22	0.16	2.40	3.32	3.05	6.37	4.22
DW18-S	0.22	0.68	0.61	1.07	0.28	0.04	0.19	2.00	2.58	2.50	5.08	1.48
DW25-S	0.19	0.43	0.43	0.92	0.24	0.16	0.14	1.40	1.97	1.94	3.91	0.89
DW28-S	0.30	0.92	0.44	1.42	0.38	0.35	0.21	2.00	3.09	2.94	6.02	2.50
DW33-S	0.32	1.01	0.75	1.96	0.62	0.45	0.44	2.20	4.04	3.70	7.74	4.44
DW36-S	0.56	1.51	0.69	1.51	0.54	0.92	0.46	2.20	4.27	4.12	8.39	1.88
DW38-S	0.39	1.70	1.16	2.45	0.85	0.17	0.67	3.60	5.69	5.29	10.98	3.69
DW40-S	0.43	1.32	0.77	2.17	0.70	1.10	0.66	2.00	4.69	4.46	9.15	2.48
DW45-S	0.47	1.52	0.96	2.11	0.67	0.87	0.74	2.60	5.06	4.88	9.94	1.82
DW51-S	0.35	1.50	1.06	1.91	0.66	0.37	0.77	3.00	4.82	4.79	9.61	0.36
DW55-S	0.91	1.98	1.22	2.08	0.65	0.49	0.93	3.60	6.20	5.67	11.86	4.45
S1-S	0.30	0.83	0.57	1.41	0.46	0.48	0.29	1.80	3.10	3.03	6.14	1.16
S2-S	0.38	0.85	0.46	1.82	0.43	0.85	0.37	1.60	3.51	3.26	6.76	3.66
S3-S	0.29	4.25	2.40	2.00	1.93	0.00	2.57	4.00	8.94	8.50	17.45	2.51
S6-S	0.18	0.51	0.53	1.03	0.19	0.07	0.11	1.80	2.25	2.17	4.42	1.88
S7-S	0.19	0.52	0.50	1.06	0.22	0.08	0.09	1.80	2.28	2.19	4.47	2.15
S8-S	0.23	0.54	0.42	1.06	0.24	0.11	0.12	1.60	2.25	2.07	4.32	4.27
BH1-S	0.32	3.17	1.02	1.54	0.80	0.00	1.61	3.40	6.06	5.81	11.87	2.10
BH2-S	0.33	3.43	0.83	1.25	0.63	0.00	1.52	3.20	5.83	5.36	11.19	4.24
BH3-S	0.49	6.58	1.46	2.25	1.49	0.00	4.42	4.20	10.79	10.10	20.89	3.26

Table 3. Characteristics of Cations and Anions in The Southeastern Section of Merapi Volcano

Samples	Ion Concentration (meq/l)								Cation	Anion	TDI	CBE (%)
	K^+	Na^+	Mg^{2+}	Ca^{2+}	SO_4^{2-}	NO_3^-	Cl^-	HCO_3^-				
DW1-SE	0.43	1.46	0.72	2.27	0.92	0.00	0.69	3.00	4.88	4.62	9.50	2.80
DW5- SE	0.89	0.97	0.58	1.20	0.35	0.44	0.42	2.20	3.63	3.42	7.05	3.05
DW15- SE	0.24	0.81	0.65	1.71	0.50	0.04	0.22	2.60	3.41	3.35	6.76	0.81
DW16- SE	0.37	1.30	0.94	2.18	1.04	0.45	0.39	2.60	4.79	4.48	9.26	3.32
DW17- SE	0.34	0.87	0.67	1.35	0.55	0.41	0.32	1.80	3.24	3.08	6.32	2.64
DW22- SE	1.52	2.74	1.81	2.99	0.40	0.01	1.39	6.80	9.06	8.60	17.66	2.65
DW25- SE	0.11	1.48	1.30	3.72	0.73	0.09	0.62	4.80	6.60	6.24	12.84	2.84
DW29- SE	0.05	0.71	0.87	1.59	0.35	0.02	0.37	2.20	3.22	2.94	6.16	4.50
DW35- SE	0.39	1.31	0.79	3.08	0.75	0.54	0.56	3.20	5.57	5.05	10.62	4.91
DW37- SE	0.54	0.98	0.62	2.79	0.37	0.16	0.33	3.80	4.92	4.66	9.59	2.72
DW39- SE	0.62	1.49	1.32	2.43	1.27	0.26	0.49	3.40	5.86	5.42	11.28	3.84
DW43- SE	0.51	1.43	0.92	2.27	0.15	0.00	0.49	4.10	5.14	4.75	9.88	3.97
S5- SE	0.20	0.72	0.51	1.58	0.36	0.14	0.18	2.20	3.02	2.89	5.90	2.24
S6- SE	0.11	0.22	0.09	0.49	0.06	0.03	0.02	0.80	0.90	0.92	1.82	-0.75
S8- SE	0.12	0.61	0.52	1.23	0.12	0.11	0.13	2.00	2.48	2.36	4.84	2.34
S12- SE	0.11	0.60	0.49	1.11	0.14	0.08	0.12	1.80	2.32	2.13	4.44	4.24
BH2- SE	0.17	0.65	0.62	1.77	0.27	0.20	0.16	2.40	3.21	3.03	6.24	2.89
BH3- SE	0.14	0.60	0.43	1.25	0.04	0.10	0.12	2.00	2.41	2.27	4.69	3.00
BH5- SE	0.20	0.67	0.49	1.51	0.07	0.16	0.20	2.20	2.87	2.64	5.51	4.23
BH7- SE	0.14	0.74	0.55	1.37	0.39	0.02	0.09	2.20	2.81	2.70	5.51	1.87
BH10- SE	0.14	1.82	0.60	0.92	0.34	0.00	0.45	2.40	3.47	3.19	6.66	4.24
BH11- SE	0.16	2.29	0.65	1.04	0.47	0.00	1.15	2.20	4.15	3.82	7.97	4.06
BH12- SE	0.14	1.82	0.60	0.88	0.52	0.00	0.62	2.20	3.44	3.34	6.78	1.48
BH13- SE	0.16	2.11	0.63	0.98	0.41	0.00	0.91	2.40	3.87	3.72	7.59	1.94

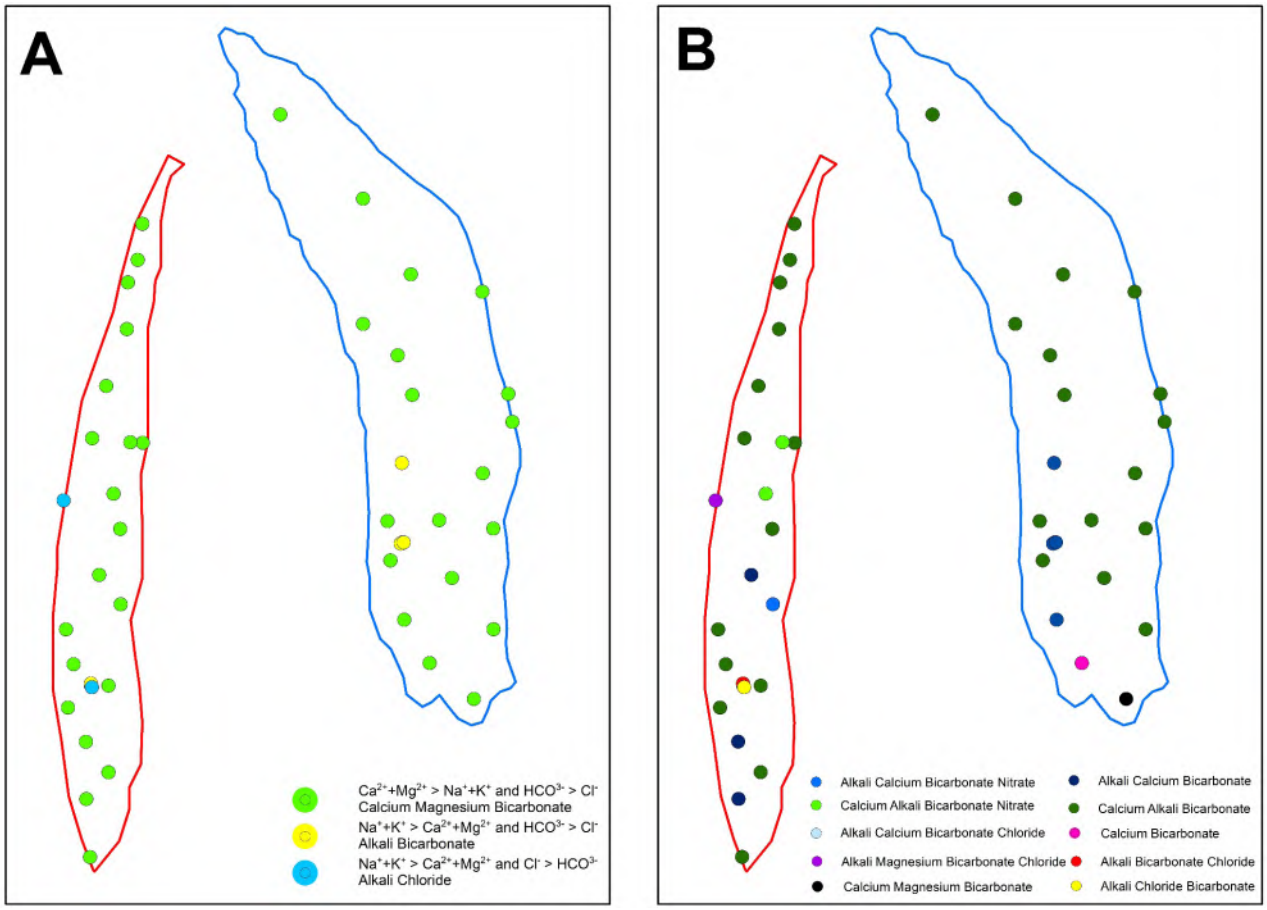

Figure 4. Distribution of Groundwater Type Based on The Piper Diagram (A) and The Kurlov Diagram (B) (Basemap Sources: Indonesian Geospatial Agency- BIG, 2004)

In flow path 7 of the volcanic foot plain's transition area, the groundwater changes to the alkali calcium bicarbonate. All samples in the southern section have large concentrations of calcium and alkali as the predominant main cations, which exceeds 25% of the total dissolved ions. The most dominant anions in the southern section are bicarbonate and chloride.

The Kurlov analysis of the southeastern section classifies the groundwater into 5 classes, namely calcium alkali bicarbonate – 16 samples, calcium bicarbonate (Ca^{2+}-HCO_3^-) – 1 sample, calcium magnesium bicarbonate (Ca^{2+}-Mg^{2+}-HCO_3^-) - 1 sample, alkali calcium bicarbonate (Na^{+}+K^{+}- Ca^{2+} - HCO_3^-) – 5 samples, and alkali calcium bicarbonate chloride (Na^{+}+K^{+}- Ca^{2+}- NO_3^--Cl^-) – 1 piece. The three groundwater classes in the southeastern part comprise alkaline bicarbonate, alkaline calcium bicarbonate, and alkaline calcium bicarbonate chloride, which are the same characteristics as the southern region. Nevertheless, the flow paths are quite different in the southeastern section. Flow path 1 is in the form of calcium alkali bicarbonate class from the upper to the lower slope of the volcano. Flow path 2, which is found in the western part of the volcanic foot, turns into the alkali calcium bicarbonate class. Similarly, those in the middle and east classes, which fall into flow path 3, are categorized into calcium alkali bicarbonate. Flow path 4 is a different class of groundwater, calcium bicarbonate, and a transitional formation area composed of tuff, tuff sandstones, and colluvial deposits in the volcanic foot plain. Flow path 5, located on structural hills, can be classified as calcium magnesium bicarbonate. All samples in the southeastern section have large concentrations of calcium and alkali as the main cations, which exceed 25% of the total dissolved ions. The most dominating anion in the southeast area is bicarbonate.

The dominant Merapi volcanic materials are from calcium alkali bicarbonate in the southern and southeastern sections. The results of different flow paths are found at Barva Volcano in Costa Rica, which comprises 3 chemical patterns of groundwater from upper, middle, and lower with differences in Mg^{2+}> Ca^{2+}, HCO_3^->NO_3^-, and HCO_3^->SO_4^{2-} (Madrigal et al., 2022). Other different facies results are found in the volcanic area of the Ethiopian Aquifer from the plateau to the plains with Ca(Mg)-Na-HCO_3, Na–Ca–HCO_3–Cl, Na–HCO_3–Cl, Na–Cl–HCO_3 composition (Furi et al ., 2012). A different pattern is also found in Italy's Cimono Volcano from the dominant upstream facies Ca ä Na > K > Mg to Ca ä Na > Mg > K at the foot of the volcano with the same value at HCO_3> > Cl > SO_4 (Piscopo et al., 2018). Other different results were also found in the upstream Mexican volcanoclastic aquifer, dominated by Ca–Na–HCO_3 >, hence the richer the valley, the more prosperous the Cl–NO–SO_4 and Na/K-HCO_3–Cl–SO_4 (Hernández-Pérez et al., 2022). Different facies patterns are also found in Hasandagi Volcano, Turkey, with upstream-downstream sequences Na–Ca–Mg–HCO_3 > Ca–Mg–HCO_3 > Ca–Na–HCO_3–Cl (Afsin et al., 2014).

In the southeast section, the increase in nitrate on calcium alkali bicarbonate and alkali calcium bicarbonate was caused by domestic sewage and septic leachate contamination in Yogyakarta City. According to preliminary studies, the problem is consistent with high nitrate levels in groundwater (Fathmawati et al., 2018; Kämpfner et al., 2021). The addition of chloride ions to alkaline chloride bicarbonate, alkaline

bicarbonate chloride, and alkaline magnesium bicarbonate chloride in the south indicates the water comes from deep groundwater. An interesting pattern is found in the southeastern section with a geological formation transition zone from volcanic rock to tuff and tuff sandstone, causing calcium bicarbonate and magnesium bicarbonate groundwater. This value is in accordance with the findings of Poetra et al. (2020), who stated that differences in geological formations and landforms affect groundwater's chemical characteristics, which can be analyzed using the Kurlov classification.

Hydrogeochemical Analysis Using the Fingerprint Diagram

The Fingerprint Diagram analysis of the southern section illustrates four groundwater systems, as shown in Figure 5. System 1, which comprises 20 samples, is characterized by concentration values of $K^+ < Mg^{2+} < Ca2^+ > Na^+$ with high HCO_3^- and low values of Cl^- and SO_4^{2-}. System 2, comprising 2 samples, is characterized by $K^+ < Mg^{2+} < Ca^{2+} < Na^+$ concentration values with high HCO_3^- and low Cl^- and SO_4^{2-} values. System 3, consisting of 1 sample, is characterized by concentration values of $K^+ < Mg^{2+} < Ca^{2+} < Na^+$ and $Cl^- > HCO_3^- > SO_4^{2-}$. Meanwhile, system 4, which consists of 1 sample, is characterized by a concentration of $K^+< Mg^{2+} > Ca^{2+} < Na^+$ with high HCO_3^- and low values of Cl^- and SO_4^{2}. The Fingerprint Diagram analysis of the southeastern section illustrates three groundwater systems, as shown in Figure 5. System 1, comprising 18 samples, is characterized by a concentration of $K^+ < Mg^{2+} < Ca2^+ > Na^+$ with high HCO_3^- and low Cl^- and SO_4^{2-} values. System 2, consisting of 4 samples, is characterized by concentrations of $K^+ < Mg^{2+} < Ca^{2+} < Na^+$ with high HCO_3^- and low Cl^- and SO_4^{2-} values. System 3, which comprises 2 samples, is characterized by concentrations of $K^+ > Mg^{2+} < Ca^{2+} > Na^+$ with high HCO_3^- and low Cl^- and SO_4^{2-} values.

Systems 1 and 2 in the southern and southeastern sections show the same pattern, characterized by volcanic aquifers with a predominance of calcium, magnesium, and alkali ions. This result is in line with previous research conducted in the southern section of the Merapi volcano (Boulom et al., 2014). Similar Fingerprint Diagram patterns have also been found in other volcanoes with a predominance of calcium, magnesium, and alkali ions (Loh et al., 2012; Hadian et al., 2016). A different pattern of fingerprint diagrams is found in the Mt Fuji Japan volcanic aquifer, which predominantly has Ca and HCO_3 from the volcano's upper-middle and the foot slopes of Mg SO_4, Na+K, and Cl values (Ono et al., 2019). The volcanoclastic aquifer of the semiarid San Juan del Río Basin was found in central Mexico with dominant ions in the form of Na+K and HCO_3+CO_3 (Hernández-Pérez et al., 2022). Different results were also found in volcanic-sedimentary aquifers in central Italy with dominant ion diagrams of Na and HCO_3+CO_3 (Vivona et al., 2007). In addition, Gibson & Hinman (2013) found another pattern in Yellowstone National Park (USA), dominant Na and Cl ions.

The geological and geomorphological characteristics differences also affect the Fingerprint Diagram analysis results (Singh & Kshetrimayum, 2021). Systems 3 and 4 found Different Fingerprint Diagrams in the southern and the southeastern area, respectively. In system 3, the chloride is more dominant than the bicarbonate, indicating that they come from deep groundwater. Meanwhile, in system 4, the alkali sodium ion is more prevalent due to the mixing process. The southeastern section in system 3 is found in the upstream area adjacent to the central facies. Its alkali, calcium, and magnesium values differ from systems 1 and 2.

Hydrogeochemical Analysis Using the Composition Diagram

The Composition Diagram analysis of the southern section of the volcano shows internal and external linear patterns, as illustrated in Figure 6. In pattern 1, the Composition Diagram is a linear line consisting of 20 samples from wells and springs. These include Deep Well BH 1 and BH 2, indicating the occurrence of shallow and deep groundwater mixing between low and high concentrations of total dissolved ions (TDI). Pattern 2 of the Composition Diagram is found in drilled wells (BH 3) and springs (S3). The BH 3 sample has the highest major ion concentrations, TDI, and EC (950 µS/cm) compared to the whole piece. The S3 sample has the second-highest major ion concentrations, TDI, and EC (850 µS/cm), with high chloride ions and drilled well BH 3 of 91.21 mg/L and 156.84 mg/L indicating that they originate from deep groundwater and aquifers. The deep well (BH 6) and the spring (S3) have higher TDI concentrations in sodium (cation) and chloride (anion). The high TDI concentrations in these sites result from a more extended water-rock interaction than dug wells and springs (Mazor, 1991).

The southeastern section in the composition diagram shows only one linear line pattern comprising shallow and deep groundwater between low and high TDI. In the southeast, groundwater experiences a blending of several types with a hydraulic relationship. The composition diagram pattern of the southern section has more variations than the southeastern. Deep and shallow aquifers can still be distinguished in the south section, with the occurrence of minimal mixing consisting of only one Merapi volcanic rock formation. A different condition is found in the southeastern section, with three formations that meet each other. However, there is no difference in the Composition Diagram pattern because the shallow and deep groundwaters have been mixing. According to Lagarde et al. (2014), composition diagrams vary from the same hill with different slope directions. Similarly, some forms of difference in diagram compositions are also found from the same plain area with varying slope directions (Rouhi & Kalantari, 2015; Berhe et al., 2017).

Different TDI analysis results comprising seawater on the Limnos Island volcanic aquifers Greece TDI were found in the freshwater mix with SO_4 and HCO_3 (Panagopoulos et al., 2013). The same results were also obtained in the volcanic island of Roccamonfona Volcano, Italy (Saroli et al., 2017), Ethiopian rift aquifers (Kebede et al., 2008), central Mexico (Afsin et al., 2014) and Portugal (Prada et al., 2005) with a linear TDI pattern with all parameters.

Harker Diagram

The analysis conducted using the Harker Diagram between rock XRF and groundwater chemistry in the southern section resulted in type 1 linear line pattern on the content of Mg – Na, Mg – Ca, and Mg – K ions, as shown in Figure 7. The linear line pattern between groundwater ion and rock chemical concentrations shows the presence of Mg-Ca, Mg-Na, and Mg-K, as indicated in Table 4. The presence of ions is influenced by volcanic lava breccia and andesite pyroclastic rocks from other volcanoes. The Harker Diagram analysis on the southeastern section also shows a linear pattern in the ion content of Mg – Na, Mg – Ca, and Mg – K, as illustrated

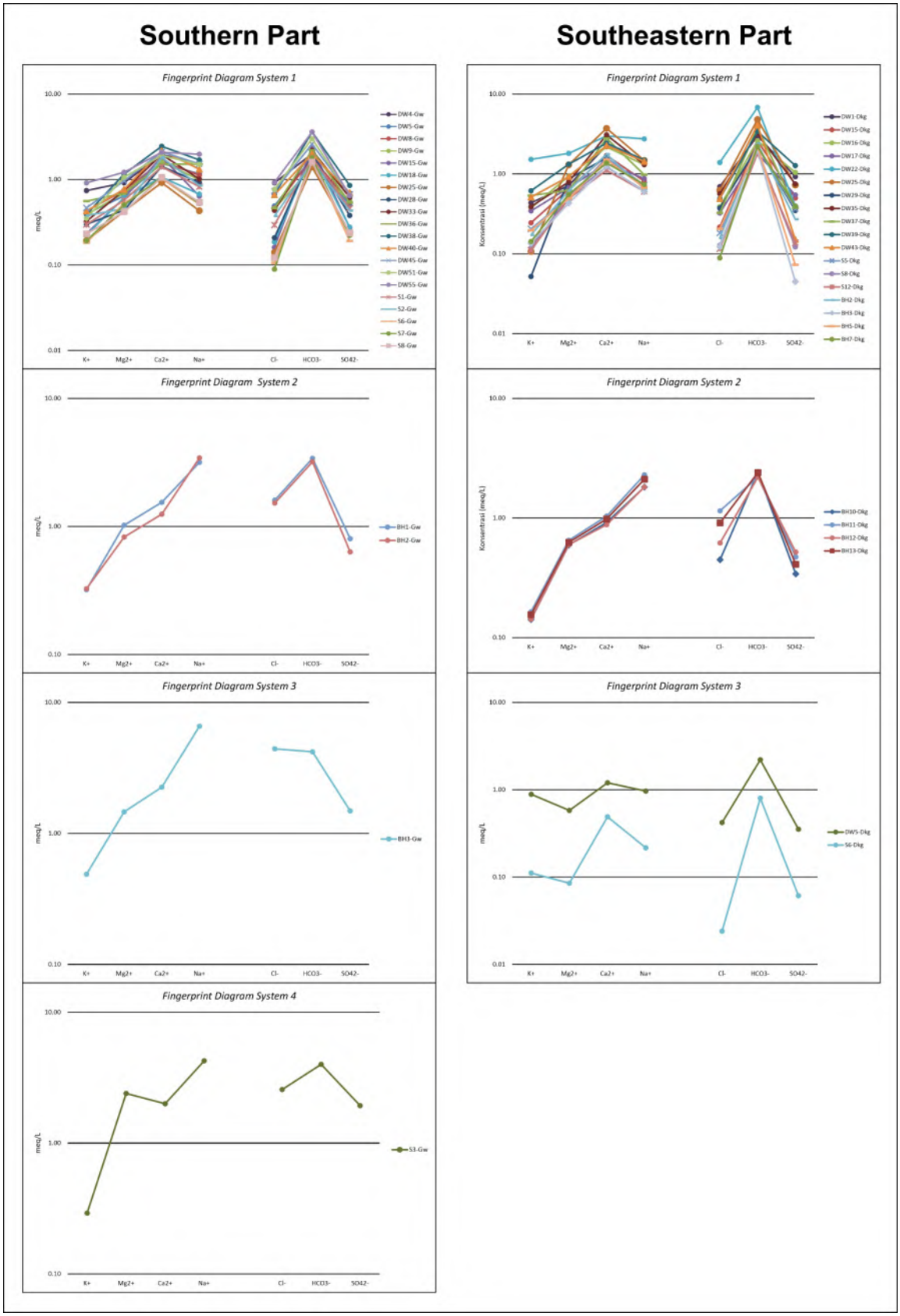

Figure 5. The Result of Analysis Using the Fingerprint Diagram Method

in Figure 7. The results also show that volcanic rocks of lava breccia and andesite-fragmented pyroclastic rocks from Merapi Volcano influence groundwater.

The same pattern in the Harker diagram is found in the Trans-Mexican Volcanic Belt area of Mexico with a grouping of Mg-Na and Mg-Ca ions (Morales-Arredondo et al., 2016). Hence, they are included in silica dissolution, one of the characteristics of groundwater influenced by volcanic rocks. The same pattern is also found in the volcanic aquifer system of Mount Vulture, southern Italy (Parisi et al., 2011); Madeira, Portugal (Prada et al., 2005); Hasandagi, Turkey (Afsin et al., 2014); and Middle Awash basin, Ethiopia (Furi et al., 2012) with groupings characteristics of Mg-Ca and Mg-Na ions.

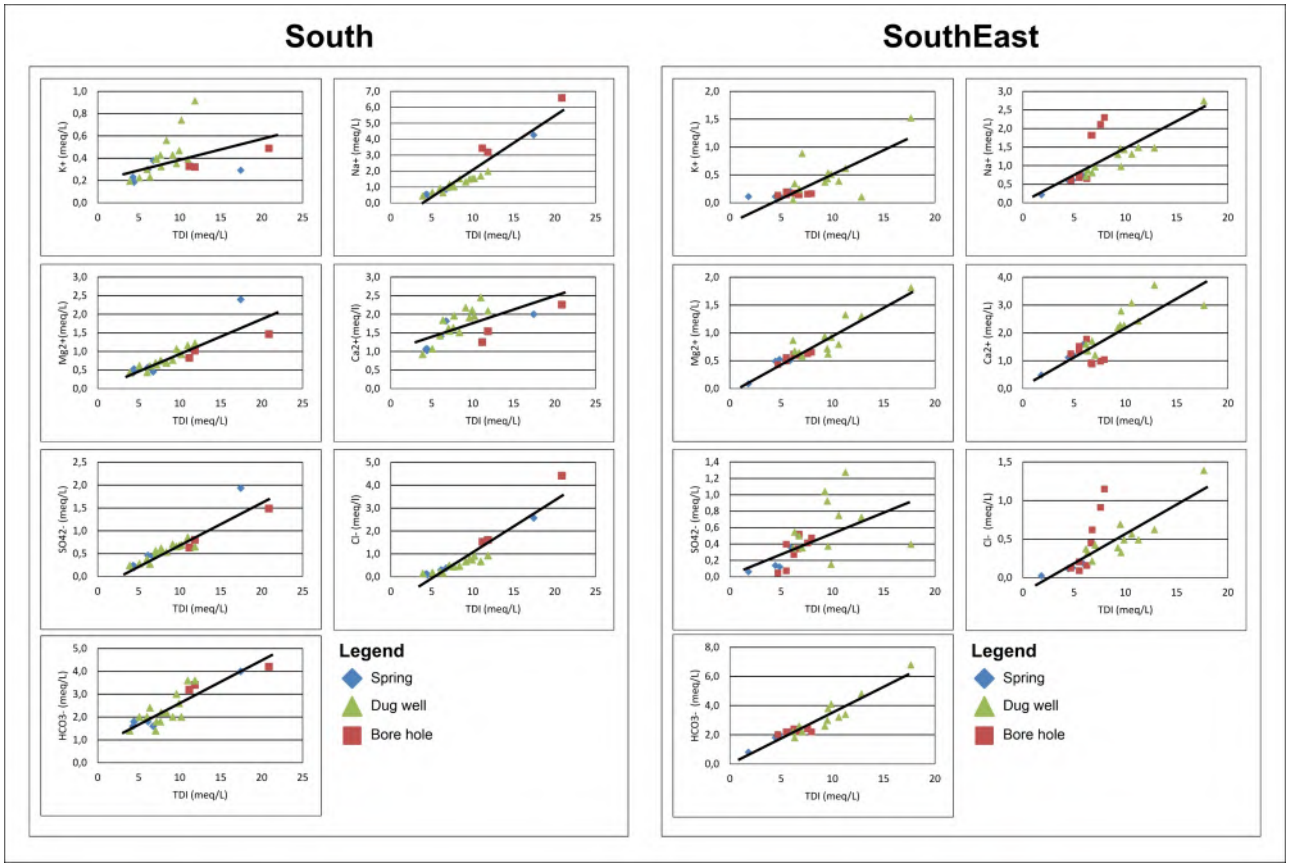

Figure 6. The Result of Analysis Using The Composition Diagram Method

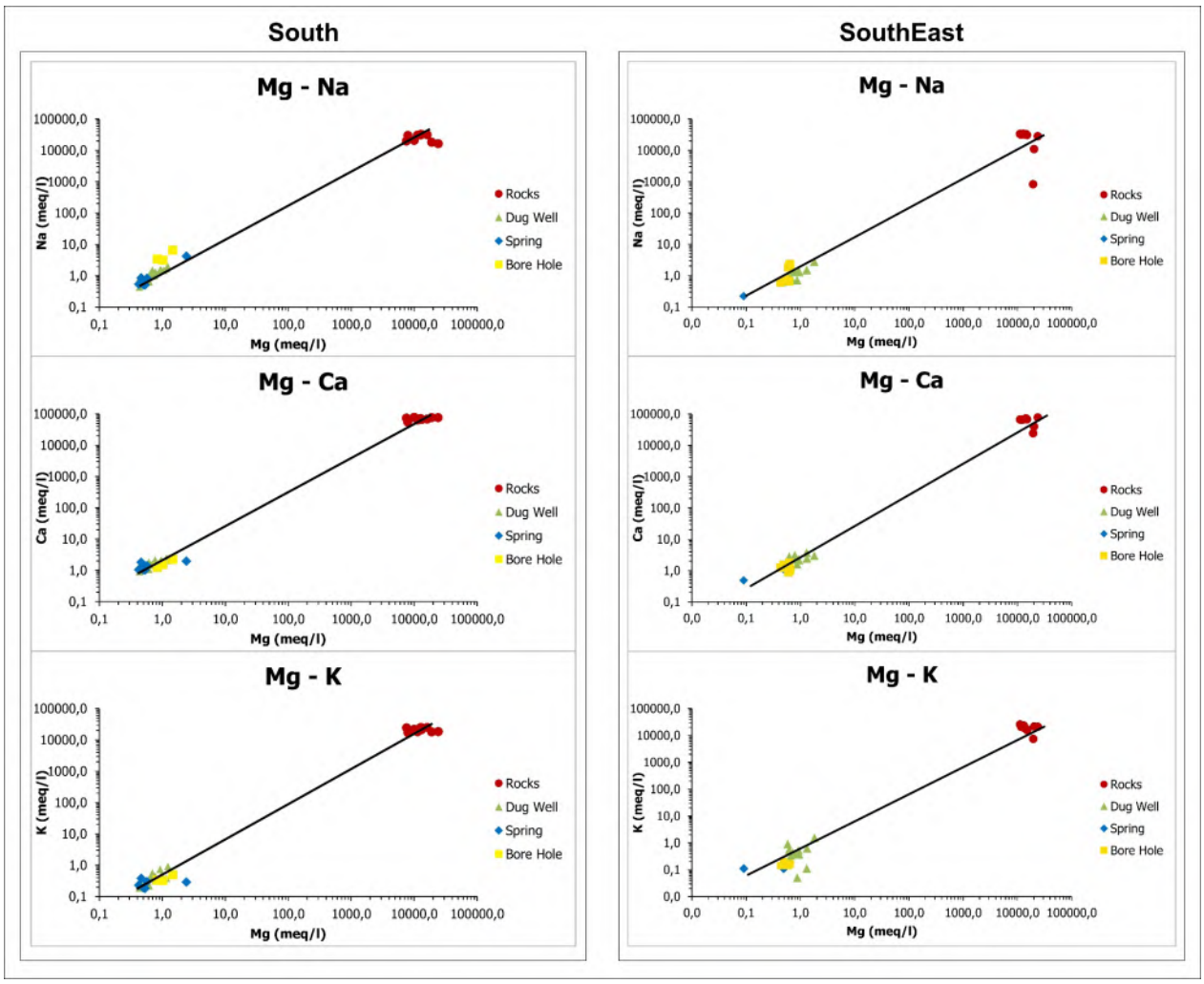

Figure 7. The results of the Harker Diagram Method

Table 4. The result of the XRF Analysis of The Southern Section of Merapi Volcano

Sample	Oxide (%)				meq/l			
	MgO	K_2O	Na_2O	CaO	MgO	K_2O	Na_2O	CaO
GW 3S	2,087	2,947	4,149	9,907	12.585	24.464	30.780	70.804
GW 4S	2,133	3,008	4,4	9,236	12.863	24.971	32.642	66.009
GW 5S	4,004	2,212	2,195	10,65	24.146	18.363	16.284	76.115
GW 6S	3,15	2,156	2,444	10,59	18.996	17.898	18.131	75.686
GW 8S	1,253	2,91	2,683	10,25	7.556	24.157	19.904	73.256
GW 9S	1,663	2,612	2,825	10,92	10.028	21.683	20.957	78.044
GW 10S	2,676	2,982	4,261	9,53	16.137	24.755	31.611	68.110
GW 11S	2,157	2,523	4,35	9,181	13.007	20.945	32.271	65.616
GW 12S	1,877	2,172	4,153	8,794	11.319	18.031	30.809	62.850
GW 14S	1,317	2,041	4,034	7,638	7.942	16.943	29.927	54.588

Table 5. The result of the XRF Analysis of The Southeastern Section of Merapi Volcano

Sample	Oxide (%)				meq/l			
	MgO	K_2O	Na_2O	CaO	MgO	K_2O	Na_2O	CaO
DKG 1 SE	3,247	0,888	0,11	3,355	19.581	7.372	816	23.978
DKG 4 SE	3,379	2,565	1,463	5,569	20.377	21.293	10.853	39.801
DKG 5 SE	1,943	2,482	4,249	9,051	11.717	20.604	31.522	64.687
DKG 9 SE	2,136	2,539	4,515	9,298	12.881	21.077	33.495	66.452
DKG 10 SE	2,178	2,788	4,397	9,408	13.134	23.145	32.619	67.238
DKG 11 SE	2,513	1,872	4,156	9,389	15.154	15.540	30.832	67.102
DKG 13 SE	2,4	2,093	4,436	10,06	14.473	17.375	32.909	71.898
DKG 14 SE	2,218	2,247	4,308	9,359	13.375	18.653	31.959	66.888
DKG 16 SE	3,939	2,493	3,775	10,82	23.754	20.696	28.005	77.330
DKG 17 SE	1,858	3,069	4,472	9,312	11.204	25.477	33.176	66.552

The southeastern section consists of two samples with the smallest XRF values of Na_2O, K_2O, and CaO, compared to the southern part, as shown in Table 5. The XRF values differ from aquifer rocks, with the two samples taken from tuffaceous sandstone and tuff capable of influencing the groundwater (Larsen et al., 1998; Maria & Hermes, 2001).

Conceptual Model of Aquifer System

The geological observation in the southern section shows that it consists of lava, breccia, pyroclastic, lahars, and debris from loose material of sand, pebble, and cobble. The geology in the southeastern part has the same lithology as the south with different transitional geological formations due to the presence of Tufan and Tuff Sandstones from the Semilir and Kebobutak Formation, as shown in Figure 8. The Semilir Formation was deposited in a shallow sea under strong currents during the Early Tertiary to Mid-Miocene (Bronto et al., 2009). Meanwhile, the Kebobutak Formation was formed during the Oligocene-Early Miocene (Surono, 2008). The uplifting process of the southern mountains caused the Kebobutak and Semilir Formations to be lifted in a range of Baturagung Hills and Yogyakarta Basin filled with Merapi volcanic materials (Mulyaningsih, 2006).

The conceptual model of the aquifer system in the study area is used to depict its relationship and connectivity with groundwater potentials. The conceptual model of the aquifer system based on hydrogeological conditions in the southern section offers three types,, as shown in Figure 9. The first is the debris flow deposits, an aquifer zone composed of loose sand, pebble, and cobble material. The debris flow deposit aquifer of Merapi Volcano is characterized by water flowing through the space between grains with high productivity and is widely distributed. The second is the aquiclude-aquifer layer of lahar and pyroclastic deposits, which consist of loose material from andesite fragments, lava deposits, and pyroclastic of Mount Merapi.

The aquiclude-aquifer layer is a zone where water flows through gaps and spaces between grains from moderate to high productivity and is widely distributed. The third is the lava flow unit, an aquifuge zone that has been adjusted according to the subsurface drill data (Hendrayana, 1993; Hendrayana && Vicente, 2013). The groundwater in the southern section flows from north to south with a contour line of groundwater elevation between 600 meters to 50 meters above sea level (masl). In comparison, the depth of the groundwater table in the study area ranges from 0.5 to 14.3 meters. The EC value and shallow groundwater temperature also show a higher trend towards the south. Based on the isotope study, the groundwater recharge area is located in the northern part of the southern section at an elevation of 650 to 1200 masl (Wijatna et al., 2008). The groundwater discharge area is located in the south section at < 650 meters.

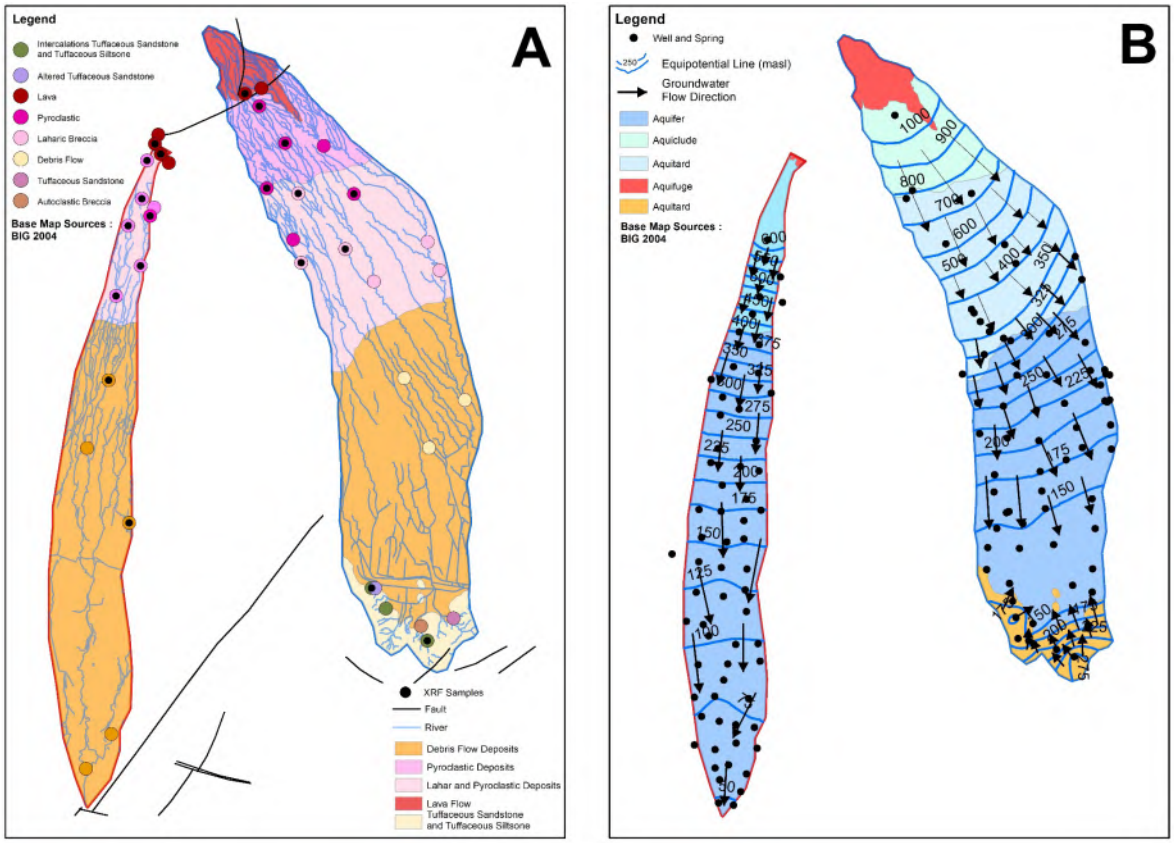

Figure 8. Lithology Distribution (A) and Hydrostratigraphy Units (B)
(Basemap Sources: Indonesian Geospatial Agency-BIG, 2004)

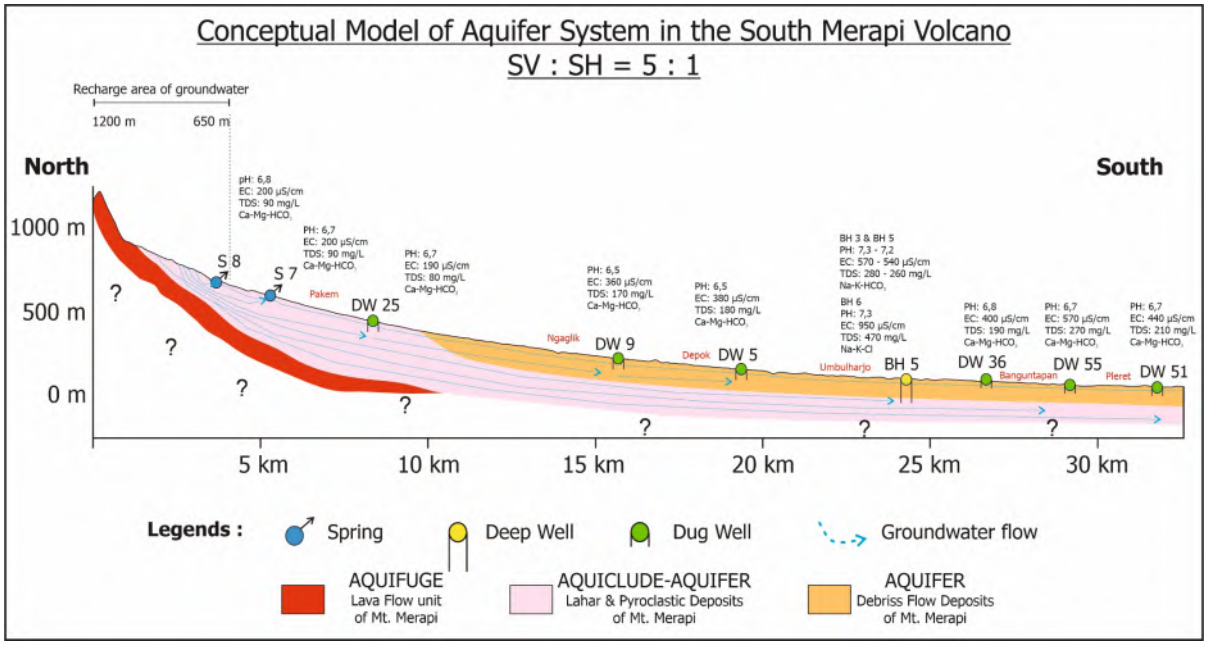

Figure 9. Conceptual Model of The Aquifer System in The Southern Section of Merapi Volcano

The conceptual model of the aquifer system based on hydrogeological conditions in the southeastern section shows 5 types of aquifers, as indicated in Figure 10. The aquifers in the southeast are typically the same as the southern, consisting of debris and lava flow deposits. However, there are differences in the aquiclude and the separated aquitard in the southeastern section. Aquitard consists of lahar deposits, lahars, and pyroclastic breccias, while aquiclude comprises pyroclastic-flow deposits. The aquitard layer consists of alternating tuffaceous sandstones and tuffaceous siltstones, characterized by groundwater flowing through the inter-grain space with average productivity and locally distributed. Selles (2014) stated that the aquifer conceptual model had been adjusted to the results of the subsurface drill data. The groundwater flow in the tuffaceous sandstone aquitard layer from the south to the north meets those from Merapi Volcano, which flows in the opposite direction. The groundwater recharge area in the southeastern section is located at an elevation.

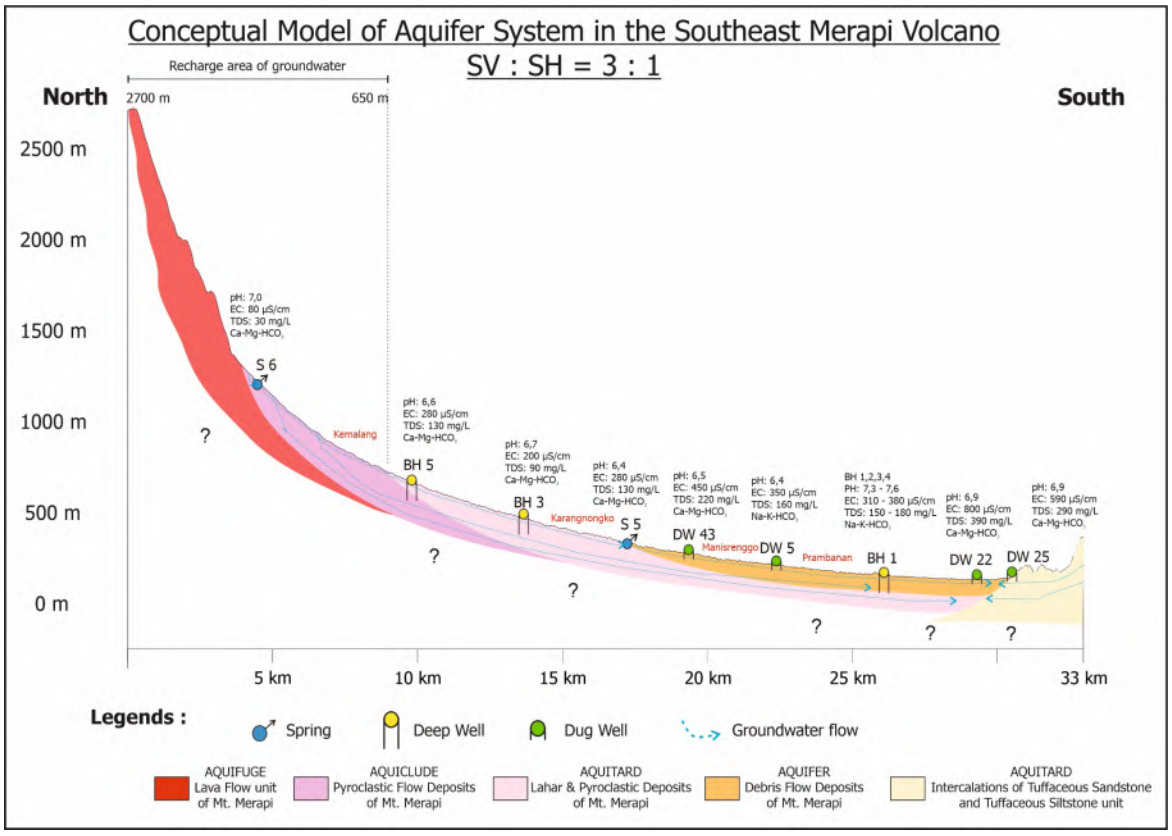

Figure 10. Conceptual Model of The Aquifer System in The Southeastern Section of Merapi Volcano

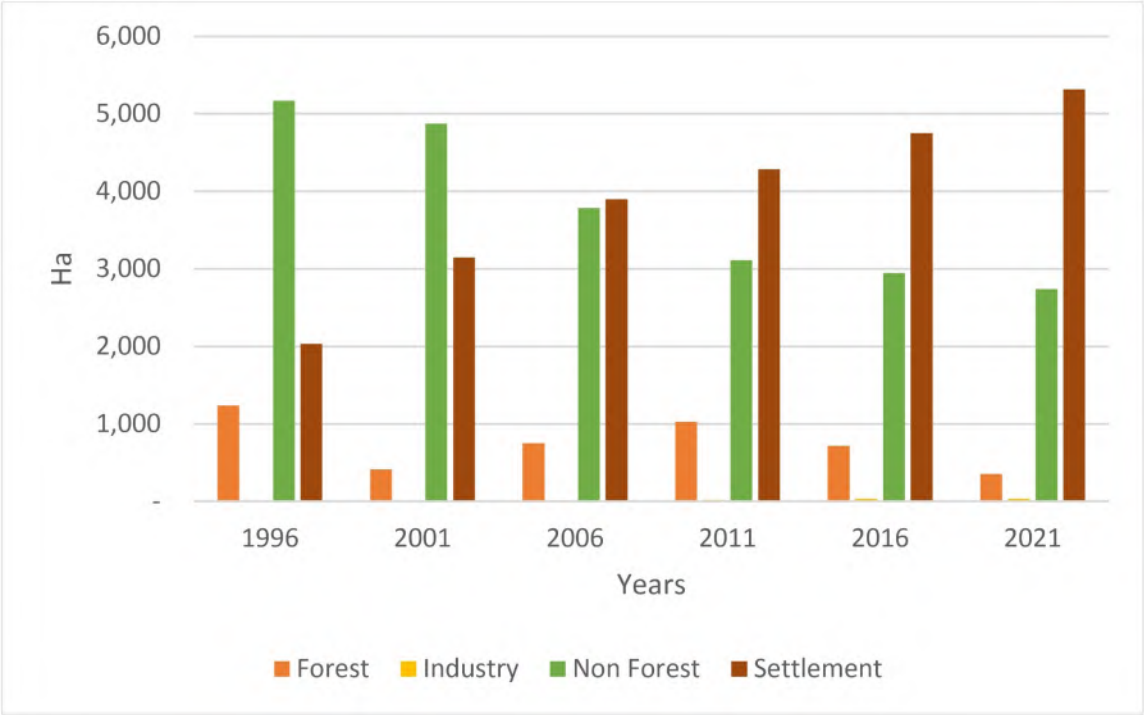

Figure 11. Land Use Change in The Southern Section of Merapi Volcano (1996 to 2021)

The two conceptual model results of the aquifer system provide convenience in determining the characteristics of hydrogeology, hydrogeochemistry, groundwater flow, recharge area, mixing, and facies. This is similar to the conceptual model pattern in Barva Volcano, Costa Rica (Madrigal et al., 2022). The same pattern was also carried out at Cimino Volcano, Italy, by making a conceptual model of the aquifer system (Piscopo et al., 2018). A similar conceptual model pattern is also applied in Hasandagi Volcano, Turkey, to determine recharge area, groundwater flow, and facies (Afsin et al., 2014). Furthermore, Furi et al. (2012) used the same pattern found in the complex volcanic aquifers of Ethiopia to depict groundwater flow. Different conceptual model patterns were carried out at Bromo Tengger Volcano to create a conceptual model based on water balance (Toulier et al., 2019).

Land Use Change, Water Use, and Groundwater Table Monitoring

The land-use change in the southern and southeastern sections shows 62%, and an insignificant increase in residential area changes, as illustrated in Figure 12. Residential areas in the southern section increased from 2,000 Ha in 1996 to 5,100 Ha in 2021, as shown in Figure 11. This increase is caused by the development of Yogyakarta City, in contrast to the southeastern section, which is less developed for housing. Land used for non-forest purposes in the southern area continues to increase yearly, while in the southeast section, the non-forest tends to fluctuate. Forest land in the southern section decreases and is more significant compared to the southeast, as shown in Figure 13. These land-use changes impact groundwater resources in the two research areas, with an increase in Industrial growth. Deep groundwater in the southern section is extracted from deep wells at 340,000 – 586,000 m^3/day, as shown in Figure 14. Several monitoring wells in the south section from 2011 to 2017 showed a declining groundwater table (Wilopo et al., 2021). Many industries are in the southeastern area, but only a few have official groundwater extraction licenses with 1,000 m^3/day of the total volume.

Land-use conversion for residential purposes affects groundwater extraction, especially for domestic needs. According to Hendrayana et al. (2021a), the groundwater measurements in the southeastern section in 2021, 2015, and 2011 were 1.5-11 meters, 1.1-10.4 meters, and 1.2-10.8 meters. In 2021, the groundwater table in this area ranged from 200-150 masl, while in 2016, it was around 130-115 masl (Lisan & Adji, 2017). The measurement in the middle part of the southeastern section in 2021 showed a range of 370-350 masl compared to 350-340 masl in 2014 (Selles, 2014). The decrease occurred along with increased groundwater use in both research areas. Its use in the southern section increased from 2011-2021 in the fisheries, worship, education, health, hotel, and restaurant sectors, as shown in Figure 15. Meanwhile, in the southeastern section, groundwater use increased in the education, health, restaurant, hotel, industry, worship, and domestic sectors from 2011-2021, as shown in Figure 15. The total water use in the southern and southeastern sections is approximately 33,000,000 m^3/year, and 21,000,000 m3/year, respectively.

4. Conclusion

The properties of groundwater chemistry in the southern and southeastern parts of Mount Merapi comprising calcium magnesium bicarbonate, alkali bicarbonate, and Akali chloride groundwater are significantly different and controlled by aquifer lithology. The results of the piper diagram of the groundwater of Mount Merapi have the same 3 patterns as other volcanoes in the world. The Kurlov classification in the southern part of Mount Merapi, comprises 7 different patterns, namely alkaline calcium bicarbonate, alkaline calcium bicarbonate nitrate, alkaline calcium bicarbonate nitrate, alkaline magnesium bicarbonate chloride, alkaline calcium, bicarbonate chloride and alkaline bicarbonate chloride.

The Fingerprint Diagram analysis of the southern section shows one additional type, more than the southeastern part, namely $K^+ < Mg^{2+} < Ca2^+ > Na^+$ with high HCO_3^- value, and low Cl^- and SO_4^{2-}, $K^+ < Mg^{2+} < Ca^{2+} < Na^+$ with high HCO_3^-, and low Cl^- and SO_4^{2-}, $K^+ < Mg^{2+} < Ca^{2+} < Na^+$ with $Cl^- > HCO_3^- > SO_4^{2-}$, and $K^+ < Mg^{2+} > Ca^{2+} < Na^+$ with high HCO_3^- and low Cl^- and SO_4^{2-}. A fingerprint Diagram of the groundwater of Merapi Volcano obtained 4 types of a different pattern from other volcanoes worldwide. The Composition Diagram of the southern section shows an internal and outside linear pattern, while the southeastern section is only a linear pattern. The Harker diagram between rock XRF and groundwater chemistry in the southern and southeastern sections shows a linear line pattern (1 type) on the content of Mg – Na, Mg – Ca, and Mg – K ions, indicating the mixing process. The Harker diagram of groundwater at Merapi Volcano has the same pattern of Mg-Ca and Mg-Na as well as several other volcanoes.

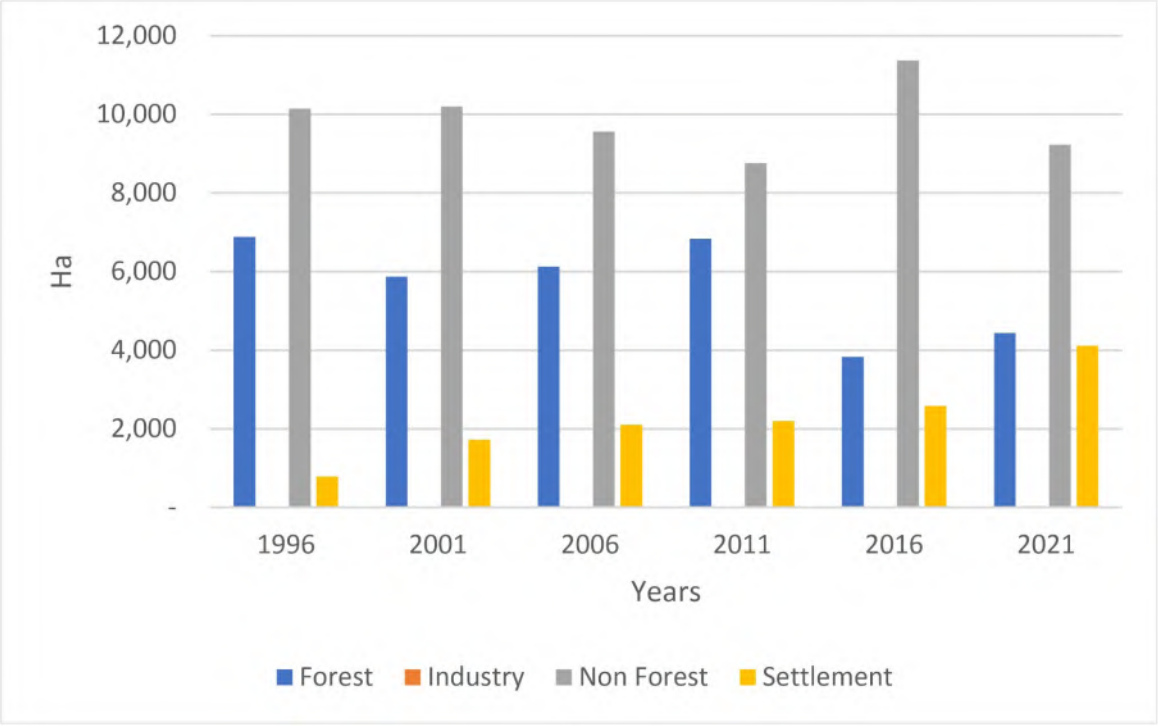

Figure 12. Land Use Change in The Southeastern Section of Merapi Volcano (1996 to 2021)

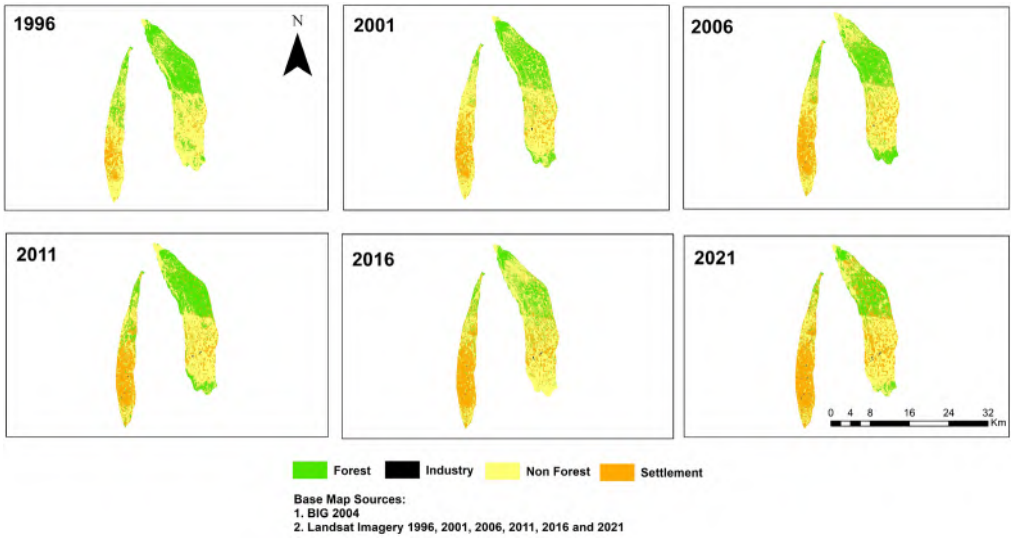

Figure 13. Land Use Change Map in Study Area (1996 to 2021)

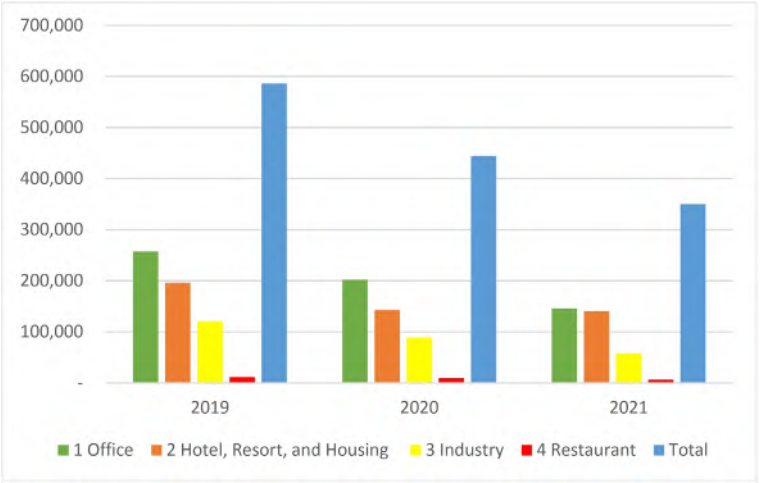

Figure 14. License Groundwater Extractions in The Southeastern Section of Merapi Volcano

Figure 15. Groundwater Use in The Study Area

The EC, pH, temperature, and TDS values in the southeastern section are higher than in the southern, especially in the downstream area, due to the presence of connate water traps. This is in addition to the mixing process of the Merapi Volcano Formation in the southeastern area and the formation of tuffaceous sandstone and tuffaceous siltstone of the Tertiary age. The southern and southeastern sections have EC values of 600-750 µS/cm, and 900-1,200 µS/cm, respectively. Several volcanic groundwaters in the world have lower and higher EC values than the study locations. For example, in the southern section, the pH values of 6.5-7, while in the southern it is 6.20-6.5. Some groundwater pH at other volcanoes in the world have the same lower and higher range as the study location. The TDS in the southern and southeastern sections ranges from 125-250 ppm and 301-600 ppm, with temperature distribution pattern of 24-30 °C. Meanwhile, others show the same lower and higher temperatures and pressures as the study location.

The geological in the southern section consists of Lava, Breccia, Pyroclastic, Lahar, and Merapi Volcano Debris units. The southeastern section's observations also show the same lithology with a transition different from the Quaternary geological formation of Semilir, and Kebobutak. The hydrostratigraphic units in the southern section consist of aquifuge (lava), aquiclude (lahar and pyroclastic deposits), and aquifer (debris flow deposits). This is in contrast with the southeastern section, which has additional aquitard from Tertiary geological formations. The land-use change in the southern section shows a dominant pattern of 62% in residential areas compared to the southeast section, with more significant groundwater extraction. The decline in the groundwater table occurs in the southern and southeastern areas. Hence, groundwater protection must be carried out at Merapi Volcano by considering land-use change, groundwater table decline, and groundwater use. It is also necessary to mitigate groundwater pollution based on groundwater quality, especially nitrate parameters.

References

Afsin, M., Allen, D. M., Kirste, D., Durukan, U. G., Gurel, A., & Oruc, O. (2014). Mixing processes in hydrothermal spring systems and implications for interpreting geochemical data: A case study in the Cappadocia region of Turkey. *Hydrogeology Journal*, 22(1), 7–23. https://doi.org/10.1007/s10040-013-1056-2

Aldrian, E., & Dwi Susanto, R. (2003). Identification of three dominant rainfall regions within Indonesia and their relationship to sea surface temperature. *International Journal of Climatology*, 23(12), 1435–1452. https://doi.org/10.1002/joc.950

Appelo, C. A. J., and Postma, D. (2005) *Geochemistry, groundwater, and pollution, 2nd edn*. Balkema Publishers, Amsterdam.

Baud, B., Lachassagne, P., Jourde, H., De Montety, V., Fadillah, A., Dörfliger, N., Hendrayana, H., and Rachmansyah, A. (2021). Preliminary conceptual model of the Arjuno Welirang hydrogeological system, and comparison with the Bromo Tengger: An illustration of the hydrogeological systems diversity in volcanic areas. *IOP Conference Series: Earth and Environmental Science*, 851(1). https://doi.org/10.1088/1755-1315/851/1/012016

Bellia, C., Gallardo, A. H., Yasuhara, M., & Kazahaya, K. (2015). Geochemical characterization of groundwater in a volcanic system. *Resources*, 4(2), 358–377. https://doi.org/10.3390/resources4020358

Berhe, A. B., Erdem Dokuz, U., and Çelik, M. (2017). Assessment of hydrogeochemistry and environmental isotopes of surface and groundwaters in the Kütahya Plain, Turkey. *Journal of African Earth Sciences*, 134: 230–240. https://doi.org/10.1016/j.jafrearsci.2017.06.015

Boulom, J., Putra, D.P.E., and Wilopo, W. (2015). Chemical composition and hydraulic connectivity of springs in the Southern section of Merapi Volcano. *Journal of Applied Geology*, 6(1): 1–11. https://doi.org/10.22146/jag.7212

BPS. (2021). *Provinsi DI Yogyakarta dan Jawa Tengah Dalam angka tahun 2021*. Badan Pusat Statistik, Jakarta.

Bremer, L.L., Elshall, A.S., Wada, C.A., Brewington, L., Delevaux, J.M.S., El-Kadi, A.I., Voss, C.I., and Burnett, K.M. (2021). Effects of land-cover and watershed protection futures on sustainable groundwater management in a heavily used aquifer in Hawai'i (USA). *Hydrogeology Journal*, 29(5): 1749–1765. https://doi.org/10.1007/s10040-021-02310-6

Bronto, S. (2009). Waduk Parangjoho dan Songputri: alternatif sumber erupsi Formasi Semilir di daerah Eromoko, Kabupaten Wonogiri, Jawa Tengah. *Indonesian Journal on Geoscience*, 4(2): 79–92. https://doi.org/10.17014/ijog.vol4no2.20091. (in Indonesian with English abstract)

BSN. (2015). *Penyusunan Neraca Spasial Sumber Daya Alam - Bagian 1: Sumber Daya Air SNI 6728.1:2015*. Badan Standardisasi Nasional, Jakarta.

Cabrera, M. C., & Custodio, E. (2004). Groundwater flow in a volcanic-sedimentary coastal aquifer: Telde area, Gran Canaria, Canary islands, Spain. *Hydrogeology Journal*, 12(3), 305–320. https://doi.org/10.1007/s10040-003-0316-y

Cahyadi, A., Haryono, E., Adji, T. N., Widyastuti, M., Riyanto, I. A., Muhammad, D. T. N., & Tastian, N. F. (2021). Rainfall variability in gunung sewu karst area, java island, indonesia. *Indonesian Journal of Forestry Research*, 8(1), 23–35. https://doi.org/10.20886/IJFR.2021.8.1.23-35

De Bélizal, E., Lavigne, F., Hadmoko, D.S., Degeai, J.P., Dipayana, G.A., Mutaqin, B.W., Marfai, M.A., Coquet, M., Mauff, B. Le., Robin, A. K., Vidal, C., Cholik, N., and Aisyah, N. (2013). Rain-triggered lahars following the 2010 eruption of Merapi volcano, Indonesia: A major risk. *Journal of Volcanology and Geothermal Research,* 261: 330–347. https://doi.org/10.1016/j.jvolgeores.2013.01.010

Delcamp, A., Roberti, G., and van Wyk de Vries, B. (2016). Water in volcanoes: evolution, storage and rapid release during landslides. *Bulletin of Volcanology*, 78(12):1-12. https://doi.org/10.1007/s00445-016-1082-8

Demlie, M., Wohnlich, S., Wisotzky, F., and Gizaw, B. (2007). Groundwater recharge, flow and hydrogeochemical evolution in a complex volcanic aquifer system, central Ethiopia. *Hydrogeology Journal*, 15(6): 1169–1181. https://doi.org/10.1007/s10040-007-0163-3

Djaeni A. (1982). *Hydrogeology map of Indonesia sheet IX Yogyakarta (Jawa)*. Geological Research and Development Centre, Bandung.

Döll, P., and Fiedler, K. (2008). Global-scale modeling of groundwater recharge. *Hydro. Earth Syst. Sci,* **12**, 863-885. www.hydrol-earth-Syst-sci.net/12/863/2008/

El-Kadi, A. I., Tillery, S., Whittier, R. B., Hagedorn, B., Mair, A., Ha, K., & Koh, G. W. (2014). Assessing sustainability of groundwater resources on Jeju Island, South Korea, under climate change, drought, and increased usage. *Hydrogeology Journal*, 22(3), 625–642. https://doi.org/10.1007/s10040-013-1084-y

Fackrell, J, K., Glenn, C.R., Thomas, D., Whittier, R., and Popp, B.N. (2020). Stable isotopes of precipitation and groundwater provide new insight into groundwater recharge and flow in a structurally complex hydrogeologic system: West Hawai'i, USA. *Hydrogeology Journal*, 28(4): 1191–1207. https://doi.org/10.1007/s10040-020-02143-9

Fathmawati, F., Fachiroh, J., Sutomo, A.H., and Putra, D.P.E. (2018). Origin and distribution of nitrate in water well of settlement areas in Yogyakarta, Indonesia. *Environmental Monitoring*

and Assessment, 190(11). https://doi.org/10.1007/s10661-018-6958-y

Fenta, M.C., Anteneh, Z.L., Szanyi, J., and Walker, D. (2020). Hydrogeological framework of the volcanic aquifers and groundwater quality in Dangila Town and the surrounding area, Northwest Ethiopia. *Groundwater for Sustainable Development*, 11:1-13. https://doi.org/10.1016/j.gsd.2020.100408

Fetter, C.W. (2000). *Applied Hydrogeology, 4nd edn*. Prentice-Hall Inc, New Jersey.

Furi, W., Razack, M., Abiye, T. A., Kebede, S., & Legesse, D. (2012). Hydrochemical characterisation of complex volcanic aquifers in a continental rifted zone: The Middle Awash basin, Ethiopia. *Hydrogeology Journal*, 20(2), 385–400. https://doi.org/10.1007/s10040-011-0807-1

Gibson, M. L., & Hinman, N.W. (2013). Mélange d'eau hydrothermale et d'eau de nappe autour des sources chaudes du Parc National de Yellowstone (USA): Hydrologie et géochimie. *Hydrogeology Journal*, 21(4), 919–933. https://doi.org/10.1007/s10040-013-0965-4

Gray, S.T., Graumlich, L.J., & Betancourt, J.L. (2007). Annual precipitation in the Yellowstone National Park region since AD 1173. *Quaternary Research*, 68(1), 18–27. https://doi.org/10.1016/j.yqres.2007.02.002

Hadian, M.S.D., Hendarmawan, Sulaksanan, N., and Azy, F.N. (2016). Hydrogeology of volcanic characterisation based on Volcanic Facies,Ground, Water Chemical Content, and Stable Isotope of Groundwater. *Proceeding. International of Chemical, Biology, and Environment Engineering.* https://DOI:10.7763/IPCBEE.2016.V94.22

Hendrayana, H., and Vicente, V.A.S (2013). [Groundwater reserve based on geometry and configuration ofaquifer sys- tem of Yogyakarta-Sleman groundwater basin] Cadangan air tanah berdasarkan geometri dan konfigurasi sistem akuifer cekungan air tanah Yogyakarta-Sleman. *Proceeding Seminar Nasional Kebumian* 6, (356–370) Teknik Geologi Universitas Gadjah Mada. https://repository.ugm.ac.id/135207/1/356-375/L03.pdf

Hendrayana., H., Nuha, A., Riyanto, I.A., and Aprimanto, B. (2021). Kajian perubahan muka air tanah di Cekungan Air tanah Yogyakarta-Sleman. *Majalah Geografi Indonesia,* 35(1), 30–44. https://doi.org/10.22146/mgi.62396 (in Indonesian with English abstract)

Hendrayana, H., Riyanto, I.A., and Nuha, A. (2020). Tingkat pemanfaatan air tanah di Cekungan Air tanah (CAT) Yogyakarta-Sleman. *Geodika: Jurnal Kajian Ilmu Dan Pendidikan Geografi,* 4(2), 127–137. https://doi.org/10.29408/geodika.v4i2.2643 (in Indonesian with English abstract)

Hendrayana, H. (1993). Hydrogeologie und Grundwassergerwinnung im Yogyakarta Becken Indonesien. *Disertation*. Arbeit der RWTH Aachen, Germany.

Herdiansyah, A.R., Hastari, N.R.F., Ramdani, H.P., and Putri, R.F,. (2020). Land use change and its impact on rice productivity in Sleman Regency 2007-2017. *IOP Conference Series: Earth and Environmental Science*, 451(1). https://doi.org/10.1088/1755-1315/451/1/012054

Hernández-Pérez, E., Levresse, G., Carrera-Hernandez, J., Inguaggiato, C., Vega-González, M., Corbo-Camargo, F., Carreón-Freyre, D. C., Billarent-Cedillo, A., Contreras, F. J. S., & Hernández, C. P. R. (2022). Geochemical and isotopic multi-tracing (δ18O, δ2H, δ13C, Δ14C) of groundwater flow dynamics and mixing patterns in the volcanoclastic aquifer of the semiarid San Juan del Río Basin in central Mexico. *Hydrogeology Journal*, 30, 2073–2095. https://doi.org/10.1007/s10040-022-02536-y

Herrera, C., and Custodio, E. (2008). Conceptual hydrogeological model of volcanic Easter Island (Chile) after chemical and isotopic surveys. *Hydrogeology Journal*, 16(7), 1329–1348. https://doi.org/10.1007/s10040-008-0316-z

Hiscock, K.M., and Bense, V.F. (2014). *Hydrogeology: principles and practices, 2nd edition*. Wiley Blackwell, London.

Hurwitz, S., Lowenstern, J. B., & Heasler, H. (2007). Spatial and temporal geochemical trends in the hydrothermal system of Yellowstone National Park: Inferences from river solute fluxes. *Journal of Volcanology and Geothermal Research*, 162(3–4), 149–171. https://doi.org/10.1016/j.jvolgeores.2007.01.003

Indonesian Geospatial Agency-BIG. (2004). Land use map of the Yogyakarta sheet, Java. Indonesian Geospatial Agency, Jakarta.

Irawan, D.E., Puradimaja, D.J., Notosiswoyo, S., and Soemintadiredja, P. (2009). Hydrogeochemistry of volcanic hydrogeology based on cluster analysis of Mount Ciremai, West Java, Indonesia. *Journal of Hydrology*, 376(1–2), 221–234. https://doi.org/10.1016/j.jhydrol.2009.07.033

Join, J.L., Folio, J.L., and Robineau, B. (2005). Aquifers and groundwater within active shield volcanoes. Evolution of conceptual models in the Piton de la Fournaise volcano. *Journal of Volcanology and Geothermal Research*, 147(1–2), 187–201. https://doi.org/10.1016/j.jvolgeores.2005.03.013

Kebede, S., Travi, Y., Asrat, A., Alemayehu, T., Ayenew, T., & Tessema, Z. (2008). Groundwater origin and flow along selected transects in Ethiopian rift volcanic aquifers. *Hydrogeology Journal*, 16(1), 55–73. https://doi.org/10.1007/s10040-007-0210-0

Kulkarni, H., Vijay Shankar, P.S., Deolankar, S.B., and Shah, M. (2004). Groundwater demand management at local scale in rural areas of India: A strategy to ensure water well sustainability based on aquifer diffusivity and community participation. *Hydrogeology Journal*, 12(2), 184–196. https://doi.org/10.1007/s10040-004-0320-x

Kämpfner, L., Rüde, T.R., and Putra, D.P.E. (2021). Characterisation of shallow groundwater chemistry in the Yogyakarta basin, Central Java. *IOP Conference Series: Earth and Environmental Science*, 851(1). https://doi.org/10.1088/1755-1315/851/1/012015

Lagarde, R.L., Boston, P.J., Campbell, A.R., Hose, L.D., Axen, G., and Stafford, K.W. (2014). Hydrogéologie du nord de la Sierra du Chiapas, Mexique: Un modèle conceptuel établi à partir de la caractérisation géochimique de sources karstiques saumâtres riches en sulfures. *Hydrogeology Journal*, 22(6), 1447–1467. https://doi.org/10.1007/s10040-014-1135-z

Larsen, L.M., Fitton, J.G., Bailey, J.C., and Kystol, J. (1998). XRF analyses of volcanic rocks from Leg 152 by laboratories in Edinburgh and Copenhagen: implications for the mobility of yttrium and other elements during alteration. *Proceedings of the Ocean Drilling Program: Scientific Results*, 152, 425–429. https://doi.org/10.2973/odp.proc.sr.152.246.1998

Lisan, A.R.K., and Adji, T.N. (2017). Identifikasi jebakan air tanah asin menggunakan pendugaan Geolistrik di wilayah Selatan Kabupaten Klaten, Jawa Tengah. *Jurnal Bumi Indonesia*, 6(2), 1-14. (in Indonesian with English abstract)

Loh, Y.S., Yidana, S.M, Asiedu, D., Akabzaa, T., and Jørgensen, N.O. (2012). Hydrochemical characterisation of groundwater in parts of the Volta Basin, Northern Ghana. *Ghana Mining Journal,* 13(1), 24-32.

Madrigal, H., Pablo, S., Gavilán, J., Vadillo, I., Alicia, P., & Sánchez, F. (2022). Discriminant model and hydrogeochemical processes for characterising preferential flow paths in four interconnected volcanic aquifers in Costa Rica. *Hydrogeology Journal*, 30, 2315-2340. https://doi.org/10.1007/s10040-022-02557-7

Mahlknecht, J., Schneider, J. F., Merkel, B. J., de Leon, I. N., & Bernasconi, S. M. (2004). Groundwater recharge in a sedimentary basin in semi-arid Mexico. *Hydrogeology Journal*, 12(5), 511–530. https://doi.org/10.1007/s10040-004-0332-6

Marfai, M.A., Cahyadi, A., Hadmoko, D.S., and Sekaranom, A.B. (2012). Sejarah letusan Gunung Merapi berdasarkan fasies gunungapi di Daerah Aliran Sungai Bedog, Daerah Istimewa Yogyakarta. *Jurnal RISET Geologi Dan Pertambangan*, 22(2),

73. https://doi.org/10.14203/risetgeotam2012.v22.59 (in Indonesian with English abstract)

Margat, J., and Gun, J. van der. (2013). *Geography of groundwater resources In groundwater around the world, a geographic synopsis*. CRC Press Taylor and Francis Group, New York.

Maria, A., and Hermes, O.D. (2001). Volcanic rocks in the Narragansett basin, Southeastern New England: Petrology and significance to early basin formation. *American Journal of Science*, 301(3), 286–312. https://doi.org/10.2475/ajs.301.3.286

Mazor, E. (1991). *Chemical and isotopic groundwater hydrology 3rd Edition*. Marcel Dekker INC, New York.

McNeely, R.N., Nelmanis, V.P., and Dwyer, L. (1979). *Water quality sourcebook, a guide to water quality parameters*. Inland Waters Directorate Water Quality Branch, Ottawa.

Minissale, A., Magro, G., Vaselli, O., Verrucchi, C., & Perticone, I. (1997). Geochemistry of water and gas discharges from the Mt. Amiata silicic complex and surrounding areas (central Italy). *Journal of Volcanology and Geothermal Research*, 79(3–4), 223–251. https://doi.org/10.1016/S0377-0273(97)00028-0

Ministry of Agriculture. (2000). *Semi detailed soil map Yogyakarta Province*. Centre of Soil and Agroclimate Research, Bandung.

Morales-Arredondo, I., Rodríguez, R., Armienta, M. A., & Villanueva-Estrada, R. E. (2016). L'origine de l'arsenic et du fluor des eaux souterraines d'un bassin volcano-sédimentaire du Mexique Central: hypothèse hydrochimique. *Hydrogeology Journal*, 24(4), 1029–1044. https://doi.org/10.1007/s10040-015-1357-8

Morales-Casique, E. (2012). Mixing of groundwaters with uncertain end-members: Case study in the Tepalcingo-Axochiapan aquifer, Mexico. *Hydrogeology Journal*, 20(3), 605–613. https://doi.org/10.1007/s10040-011-0826-y

Mulligan, B.M., Ryan, M.C., and Cámbara, T.P. (2011). Delineating volcanic aquifer recharge areas using geochemical and isotopic tools. *Hydrogeology Journal*, 19(7), 1335–1347. https://doi.org/10.1007/s10040-011-0766-6

Mulyaningsih, S. (2006). Perkembangan geologi pada Kuarter Awal sampai masa sejarah di Dataran Yogyakarta. *Indonesian Journal on Geoscience*, 1(2), 103–113. https://doi.org/10.17014/ijog.vol1no2.20065. (in Indonesian with English abstract)

Nasr, M., and Zahran, H.F. (2014). Using of pH as a tool to predict the salinity of groundwater for irrigation purpose using artificial neural network. *Egyptian Journal of Aquatic Research*, 40(2), 111–115. https://doi.org/10.1016/j.ejar.2014.06.005

Ohmer, M., Liesch, T., Geoppert, N., Goldscheider, N. (2017). On the optimal selection of interpolation methods for groundwater contouring: an example of propagation of uncertainty regarding inter-aquifer exchange. *Advance in Water Resources,* 109, 121–132.

Ono, M., Machida, I., Ikawa, R., Kamitani, T., Oyama, K., Muranaka, Y., Ito, A., & Marui, A. (2019). Regional groundwater flow system in a stratovolcano adjacent to a coastal area: a case study of Mt. Fuji and Suruga Bay, Japan. *Hydrogeology Journal*, 27(2), 717–730. https://doi.org/10.1007/s10040-018-1889-9

Oyedotun, T.D.T. (2018). X-ray fluorescence (XRF) in the investigation of the composition of earth materials: a review and an overview. *Geology, Ecology, and Landscapes*, 2(2), 148–154. https://doi.org/10.1080/24749508.2018.1452459

Panagopoulos, G., Panagiotaras, D., & Giannoulopoulos, P. (2013). Groundwater Quality Assessment of the Limnos Island Volcanic Aquifers, Greece. Water *Environment Research*, 85(5), 422–433. https://doi.org/10.2175/106143012x13373575831439

Pannekoek, A.J. (1949). *Outline of the geomorphology of Java*. S.I Publisher, Leiden.

Parisi, S., Paternoster, M., Kohfahl, C., Pekdeger, A., Meyer, H., Hubberten, H. W., Spilotro, G., & Mongelli, G. (2011). Groundwater recharge areas of a volcanic aquifer system inferred from hydraulic, hydrogeochemical and stable isotope data: Mount Vulture, southern Italy. *Hydrogeology Journal*, 19(1), 133–153. https://doi.org/10.1007/s10040-010-0619-8

Piscopo, V., Armiento, G., Baiocchi, A., Mazzuoli, M., Nardi, E., Piacentini, S. M., Proposito, M., & Spaziani, F. (2018). Role of high-elevation groundwater flows in the hydrogeology of the Cimino volcano (central Italy) and possibilities to capture drinking water in a geochemically contaminated environment. *Hydrogeology Journal*, 26(4), 1027–1045. https://doi.org/10.1007/s10040-017-1718-6

Piscopo, V., Lotti, F., Formica, F., Lana, L., & Pianese, L. (2020). Groundwater flow in the Ischia volcanic island (Italy) and its implications for thermal water abstraction. *Hydrogeology Journal*, 28(2), 579–601. https://doi.org/10.1007/s10040-019-02070-4

Poetra, R.P., Adji, T.N., Santosa, L.W., and Khakhim, N. (2020). Hydrogeochemical conditions in groundwater systems with various geomorphological units in Kulonprogo Regency, Java Island, Indonesia. *Aquatic Geochemistry*, 26(4), 421-454. https://doi.org/10.1007/s10498-020-09384-w

Prada, S. N., da Silva, M. O., & Cruz, J. V. (2005). Groundwater behaviour in Madeira, volcanic island (Portugal). *Hydrogeology Journal*, 13(5–6), 800–812. https://doi.org/10.1007/s10040-005-0448-3

Purnomo, B.J, and Pichler, T. (2015). Geothermal systems on the island of Bali, Indonesia. *Journal of Volcanology and Geothermal Research*, 304, 349–358. https://doi.org/10.1016/j.jvolgeores.2015.09.016

Putra, D.P.E. (2015). Evolution of groundwater chemistry on the shallow aquifer of Yogyakarta City urban area. *Journal of Applied Geology*, 3(2), 116–124. https://doi.org/10.22146/jag.7188

Qian, J. H., Robertson, A. W., & Moron, V. (2010). Interactions among ENSO, the monsoon, and diurnal cycle in rainfall variability over Java, Indonesia. *Journal of the Atmospheric Sciences*, 67(11), 3509–3524. https://doi://0.1175/2010JAS3348.1

Rahardian, A., and Buchori, I. (2016). Dampak perubahan penggunaan lahan terhadap limpasan permukaan dan laju aliran puncak Sub DAS Gajahwong hulu Kabupaten Sleman. *Jurnal Pembangunan Wilayah & Kota*, 11(4), 127. https://doi.org/10.14710/pwk.v12i2.12890. (in Indonesian with English abstract)

Rahardjo, W., Sukandarrumidi, Rosidi, H.M.D. (1995). *Geological map of the Yogyakarta sheet, Java*. Geological Research and Development Centre, Bandung.

Rahardjo, W. (2000). Tinjauan geologi dan paleogeografi daerah dataran Gantiwarno, antara Prambanan – Klaten, Jawa Tengah. *Proceedings of Indonesian Association of Geologists, the 29th Annual Convention, Bandung*. (in Indonesian with English abstract)

Revil, A., Finizola, A., Sortino, F., and Ripepe, M. (2004). Geophysical investigations at Stromboli volcano, Italy: Implications for groundwater flow and paroxysmal activity. *Geophysical Journal International*, 157(1), 426–440. https://doi.org/10.1111/j.1365-246X.2004.02181.x

Riyanto, I.A., Widyastuti, M., Cahyadi, A., Agniy, R.F, and Adji, T.N. (2020). Groundwater Management Based on Vulnerability to Contamination in the Tropical Karst Region of Guntur Spring, Gunungsewu Karst, Java Island, Indonesia. *Environmental Processes*, 7(4), 1277–1302. https://doi.org/10.1007/s40710-020-00460-5

Rouhi, H., and Kalantari, N. (2015). Chemical composition of groundwater and brines as a result of hydrogeochemical processes in arid zones: an example from Albaji plain, Khuzestan, Iran. *Arabian Journal of Geosciences*, 8(10), 8361–8372. https://doi.org/10.1007/s12517-015-1818-3

Santosa, L.W., and Sutikno. (2006). Geomorphological Approach for Regional Zoning In The Merapi Volcanic Area. *Indonesian*

Journal of Geography, 38(1), 53–68. https://doi.org/10.22146/indo.j.geog,2235

Sarminingsih, A., Siwi, H.D., Sutrisno, E., and Zaman, B. (2018). Evaluation the water availability in the Dengkeng River due to land use and climate changes. *E3S Web of Conferences, 73*. https://doi.org/10.1051/e3sconf/20187303008

Saroli, M., Lancia, M., Albano, M., Casale, A., Giovinco, G., Petitta, M., Zarlenga, F., & dell'Isola, M. (2017). Un modèle conceptuel hydrogéologique de la zone hydrothermale de Suio (Centre de l'Italie). *Hydrogeology Journal*, 25(6), 1811–1832. https://doi.org/10.1007/s10040-017-1549-5

Selles, A., Deffontaines, B., Hendrayana, H., and Violette, S. (2015). The eastern flank of the Merapi volcano (Central Java, Indonesia): Architecture and implications of volcaniclastic deposits. *Journal of Asian Earth Sciences*, 108, 33–47. https://doi.org/10.1016/j.jseaes.2015.04.026

Selles, A. (2014). Multi-disciplinary study on the hydrogeological behaviour of the eastern flank of the Merapi volcano, Central Java. *PhD thesis*. Université Pierre et Marie Curie, Paris.

Siebert, S., Burke, J., Faures, J.M., Frenken, K., Hoogeveen, J., Döll, P., and Portmann, F.T. (2010). Groundwater use for irrigation - A global inventory. *Hydrology and Earth System Sciences*, 14(10), 1863–1880. https://doi.org/10.5194/hess-14-1863-2010

Singh, L.P., and Kshetrimayum, K.S. (2021). Evaluation of spatial characteristics of groundwater hydrochemical constituents across different geomorphic units of the Imphal Valley in Northeast India. *Sustainable Water Resources Management*, 7(4), 1–18. https://doi.org/10.1007/s40899-021-00533-9

Sophocleous, M. (2005). Groundwater recharge and sustainability in the High Plains aquifer in Kansas, USA. *Hydrogeology Journal*, 13(2), 351–365.https://doi.org/10.1007/s10040-004-0385-6

Sophocleous, M. (2010). Revue critique: Pratiques, défis et innovations dans le domaine des de la gestion des eaux souterraines de l'aquifère des Grandes Plaines (High Plains), aux Etats Unis d'Amérique - Leçons et recommandations. *Hydrogeology Journal*, 18(3), 559–575. https://doi.org/10.1007/s10040-009-0540-1

Sugiyama, A., Masuda, S., Nagaosa, K., Tsujimura, M., and Kato, K. (2018). Tracking the direct impact of rainfall on groundwater at Mt. Fuji by multiple analyses including microbial DNA. Biogeosciences, 15, 721-732. https://doi.org/10.5194/bg-2016-78,2016.

Surono, S. (2008). Litostratigrafi dan sedimentasi Formasi Kebo dan Formasi Butak di Pegunungan Baturagung, Jawa Tengah Bagian Selatan. *Indonesian Journal on Geoscience*, 3(4), 183–193. https://doi.org/10.17014/ijog.vol3no4.20081. (in Indonesian with English abstract)

Todd, D.K., and Mays, L.W. (2005). *Groundwater Hydrology, 3rd edn*. John Wiley and Sons Inc, Hoboken.

Toulier, A., Baud, B., de Montety, V., Lachassagne, P., Leonardi, V., Pistre, S., Dautria, J.M., Hendrayana, H., Miftakhul, F.M.H, Satrya, M.A., Beon, O., and Jourde, H. (2019). A multidisciplinary study with quantitative analysis of isotopic data for assessing the recharge and functioning of volcanic aquifers: Case of Bromo-Tengger volcano, Indonesia. *Journal of Hydrology*, 26(2019), 1-30. https://doi.org/10.1016/j.ejrh.2019.100634

UNESCO. (2004). *Resources of the World and their use, IHP-VI series on groundwater No. 6*. United Nations, Paris.

Ureta, G,. Németh, K., Aguilera, F., and González, R. (2020). Features that favour the prediction of the emplacement location of maar volcanoes: A case study in the central andes, northern chile. *Geosciences*, 10(12), 1–25. https://doi.org/10.3390/geosciences10120507

van Bemmelen, R.W. (1949). *The geology of Indonesia, general geology of Indonesia and adjacent archioelagoes, 2nd edn*. Elsevier, The Hague.

Verstappen, H.Th. (2000). *Outline of the geomorphology of Indonesia: a case study on tropical geomorphology of a tectigene region*. ITC Publication, Enschede.

Vivona, R., Preziosi, E., Madé, B., & Giuliano, G. (2007). Occurrence of minor toxic elements in volcanic-sedimentary aquifers: A case study in central Italy. *Hydrogeology Journal*, 15(6), 1183–1196. https://doi.org/10.1007/s10040-007-0169-x

Wijatna, A.B., Sudarmadji, Sunarno., and Hendrayana, H. (2008). Tracing the origin of spring water by using environmental isotopes in the southern section of Merapi Volcano. *ASEAN Engineering Journal*, 2(2), 118–130.

Wilopo, W., Putra, D.P.E., and Hendrayana, H. (2021). Impacts of precipitation, land use change and urban wastewater on groundwater table fluctuation in the Yogyakarta-Sleman Groundwater Basin, Indonesia. *Environmental Monitoring and Assessment*, 193(2). https://doi.org/10.1007/s10661-021-08863-z

Wredaningrum, I., and Sudibyakto (2014) Analisis perubahan zona agroklimat daerah istimewa yogyakarta ditinjau dari klasifikasi iklim menurut oldeman. *Jurnal Bumi Indonensia*, 3(4),1-10. (in Indonesian with English abstract)

Zaennudin, A. (2010). The characteristic of eruption of Indonesian active volcanoes in the last four decades. *Jurnal Lingkungan Dan Bencana Geologi*, 1(2), 113–129.